

Metamorphism, magmatism, and exhumation history of the Tavşanlı Zone, NW Turkey: new petrological constraints

Şenel ÖZDAMAR^{1*}, Gürsel SUNAL¹, Muhterem DEMİROĞLU¹, Cenk YALTIRAK¹, Mehmet Zeki BİLLOR², Stoyan GEORGIEV³, Willis HAMES², Istvan DUNKL⁴, Halil Can AYDIN¹

¹Department of Geological Engineering, Faculty of Engineering, İstanbul Technical University, İstanbul, Turkey

²Department of Geosciences, College of Sciences and Mathematics, Auburn University, Auburn, Alabama, USA

³Department of Geochemistry and Petrology, Bulgarian Academy of Sciences, Sofia, Bulgaria

⁴Geoscience Center, University of Göttingen, Göttingen, Germany

Received: 19.12.2017 • Accepted/Published Online: 29.04.2018 • Final Version: 24.07.2018

Abstract: The Tavşanlı Zone (TZ) is a high-pressure/low-temperature metamorphic belt representing subduction and exhumation between the Sakarya Zone and the Afyon-Bolkardağ Zone in western Anatolia. This paper provides new and precise geological data including whole-rock and mineral chemistry, phengite ⁴⁰Ar/³⁹Ar ages, zircon laser ablation ICP-MS U-Pb, and apatite (U-Th)/He thermochronological information for a region of the Sivrihisar metamorphic complex that has been less studied than other regions of the TZ. This region comprises Permo-Carboniferous metamorphic units, Eocene granodiorite and microgranodiorite, terrestrial clastics, and Holocene alluvium. The mineral assemblage of the granite-gneiss contains quartz, plagioclase, K-feldspar, microcline, muscovite, and rare biotite and garnet, while the blueschist comprises plagioclase, white mica, biotite, Na-amphibole, and garnet that are considered to represent greenschist and blueschist facies metamorphism, respectively. We estimate the peak metamorphic conditions for schists of the Permo-Carboniferous metamorphics and associated rocks as T = 303–484 °C and P ≥ 10 kbar. This high-pressure event occurred at ca. 83 Ma, indicated by a well-defined ⁴⁰Ar/³⁹Ar plateau age for phengite. Laser ablation ICP MS U-Pb analyses of euhedral or subeuhedral magmatic zircons from previously unknown microgranodiorite, intruding the metamorphic rocks, yield an Eocene (50 Ma) age. The new results are interpreted to indicate that lithospheric collision and northward subduction beneath the Sakarya Zone occurred between 83 and 50 Ma. Apatite crystals separated from microgranodiorite yield (U-Th)/He ages consistent with cooling of the Tavşanlı Zone to ~65 °C by ~38 Ma.

Key words: Phengite ⁴⁰Ar/³⁹Ar, zircon ICP-MS U-Pb, apatite (U-Th)/He, Tavşanlı Zone, Neo-Tethys, Gondwanaland

1. Introduction

The study area (Figure 1) is located in a region of the Sivrihisar metamorphic complex that has been less studied than other regions of the Tavşanlı Zone (TZ). It is situated in the Anatolide-Tauride Block (ATB), which includes the TZ, Afyon-Bolkardağ Zone (ABZ), and Menderes Massif (MM), 50–60 km wide and 250 km long (Figure 1), and comprises subduction-related blueschist and greenschist facies metamorphic rocks formed during the Late Cretaceous convergent history of this region. The constituent lithologies of this region are mainly Paleozoic metamorphic rocks, Eocene intrusive rocks and microgranodiorite, Neogene sedimentary rocks, and recent alluvium (Figures 2 and 3).

In the northern part of this zone, the Sakarya Zone (SZ) is an east-west trending belt that is 100–200 km wide and comprises several pre-Alpine terranes in its basement

as tectonic assemblages representing a completely different geological history in the northern part of Gondwana (Figure 4). The tectonostratigraphic units of this zone are remnants of Variscan and Cimmerian continental and oceanic assemblages. The lower part of the SZ is Early Jurassic in age, followed by a relatively continuous succession of Jurassic-Cretaceous platform sediments. Continental slope deposits from the Late Cretaceous onward dominate this succession, with upper sections that include flysch-type deposits and ophiolitic blocks (Göncüoğlu et al., 1997).

In the south of this zone, the ABZ, which is structurally below the TZ, records a low-grade high-pressure/low-temperature (HP/LT) metamorphism (Okay, 1984; Robertson et al., 2009; Özdamar et al., 2012). The timing of this metamorphism is constrained by Paleogene intrusives (Candan et al., 2005; Özdamar et al., 2013; Pourteau

* Correspondence: ozdamarse@itu.edu.tr

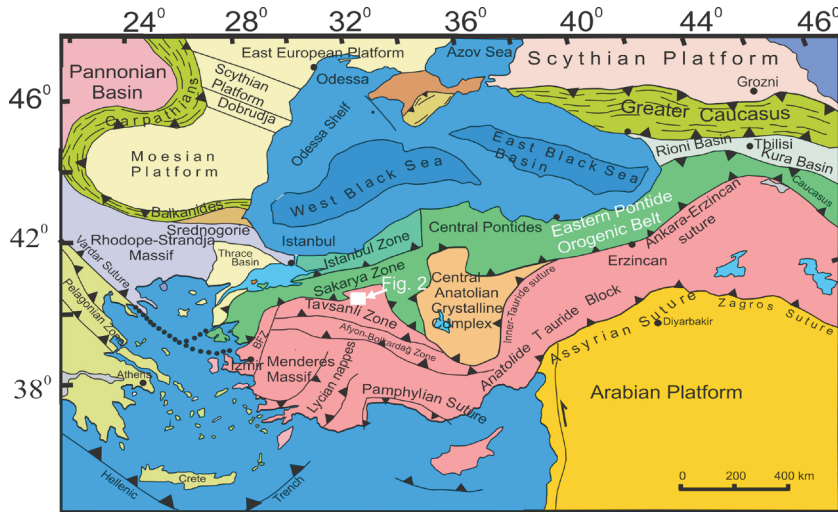


Figure 1. Regional tectonic setting of Turkey with main blocks in relation to the Afro-Arabian and Eurasian plates (simplified from Okay and Tüysüz, 1999).

et al., 2013) and by the Late Paleocene–Early Eocene sedimentary cover in the west of the region.

The high-grade metamorphic rocks of the TZ have been studied by several authors (Şengör and Yılmaz, 1981; Okay, 1984; Okay, 1989; Sherlock et al., 1999; Robertson et al., 2009; Okay and Whitney, 2011). During the Late Cretaceous, the subduction trench collided with the ATB, burying metamorphic trench sequences with blueschist-facies conditions (Okay, 2002). These HP/LT metamorphic rocks were exhumed in Paleocene time (Okay and Kelley, 1994; Sherlock et al., 1999).

The tectonic evolution of the TZ from Late Mesozoic to Early Cenozoic continues to be a subject of debate because of its complexity and the lack of critical constraints from systematic geological, geochemical, and geochronological data. Our field-based study in the Sivrihisar area of the TZ yields new geochemical and precise geochronological data useful to (1) provide critical structural data, cross-sections, petrological observations, and P-T estimates for this important zone; (2) constrain the timing of the metamorphism, magmatism, and exhumation history of the TZ; and (3) understand the regional geodynamic evolution of the Neo-Tethys Ocean in the northern part of Gondwana.

2. Geological framework

In western Anatolia, the ATB is composed of metamorphic and nonmetamorphic units (Figure 1; Özdamar et al., 2013). The TZ is one of the most important metamorphic belts of this block and extends NW to SE between the SZ and the ABZ (Özdamar et al., 2012). The lithostratigraphy of the TZ has been studied and established by several authors (Okay, 1984; Okay and Kelley 1994; Sherlock et al., 1999; Okay, 2002). The well-defined lithostratigraphy

of this zone can be separated into two tectonic units: a lower coherent blueschist sequence and the overlying Cretaceous accretionary complex (Okay, 2002). The lower coherent sequence includes a metamorphic assemblage that comprises graphitic schists and phyllites with jadeite, glaucophane, lawsonite, and chloritoid (Okay and Kelley, 1994). Marbles of several kilometers in thickness conformably overlay the metapelitic sequence (Okay, 1986). These marbles gradually pass into an overlying thick metavolcano-sedimentary sequence with intercalations of metabasite, metachert, and metapelite. Blueschist facies minerals are well preserved in all units (Okay, 1986). The Cretaceous accretionary complex is made up of imbricated and strongly tectonized serpentinites, pelagic shales and limestones, basalts, and radiolarian cherts. This complex underwent incipient blueschist facies metamorphism that developed aragonite, sodic pyroxene, and lawsonite in the veins and amygdules of metabasalts. The Cretaceous accretionary complex is tectonically overlain by large ophiolitic slabs consisting predominantly of peridotite with rare gabbroic veins (Okay, 1986). These ophiolites have not experienced Alpine HP/LT metamorphism and represent the obducted oceanic lithosphere of the Neo-Tethyan Ocean (Okay, 1984).

The studied area is located at Sivrihisar in the Eskişehir area of the TZ, NW Turkey. In this area, five main lithostratigraphic units are recognized: Permo-Carboniferous Göktepe and Kertek metamorphic units; Eocene Sivrihisar granodiorite and its hypabyssal equivalents; Miocene Hisar, Çakmak, and Mercan units; Pleistocene Kepen terrestrial clastics; and Holocene alluvium (Kulaksız, 1981; Whitney, 2002; Örgün et al., 2005; Whitney and Davis, 2006; Demiroğlu, 2008; Figures 2 and 3). The metamorphic Göktepe and Kertek units are

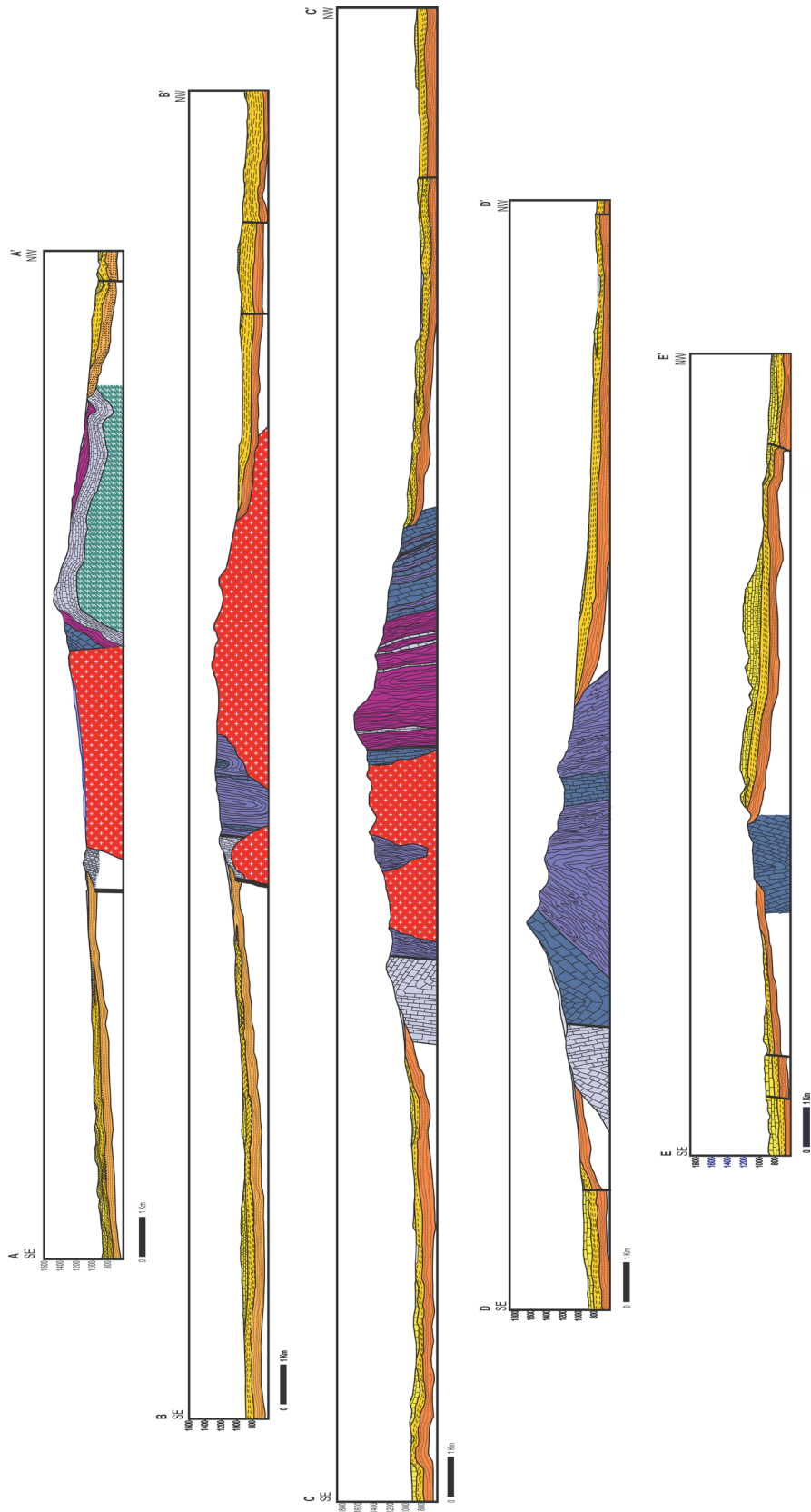


Figure 3. Schematic cross-sections of the Sivrihisar area showing the gross scale structures and the tectonostratigraphic units.



Figure 4. The map of Eurasia showing Laurasia and Gondwanaland and suture zones in Turkey (modified from Okay, 1989).

accelerating voltage, 5–15 mA current, variable electron beam diameter, and 10–20 s counting time per element. Spectrometers were automated with dQANT software from Geller Microanalytical Laboratory.

3.2. Major and trace element analyses

Representative rock samples, crushed in an agate mill to ~200 mesh, underwent whole-rock chemical analyses at ACME Analytical Laboratories, Canada. Pulverized whole-rock samples were mixed with $\text{LiBO}_2/\text{Li}_2\text{B}_4\text{O}_7$ flux and fused in a furnace. The cooled bead was dissolved in ACS grade nitric acid and analyzed by ICP and/or ICP-MS. Analytical precision, as calculated from replicate analyses, is within 0.01–0.04 wt.% for the major elements and 0.01–8.0 ppm for trace elements.

3.3. $^{40}\text{Ar}/^{39}\text{Ar}$ dating

To evaluate the timing of the geological events, $^{40}\text{Ar}/^{39}\text{Ar}$ geochronology was carried out on phengite samples in the Auburn University Noble Isotope Mass Analysis Laboratory (ANIMAL). Two muscovite schists samples were selected for $^{40}\text{Ar}/^{39}\text{Ar}$ dating after detailed petrographical study, microprobe analysis, and study of the field relations to other lithologies. Muscovite-bearing metamorphosed rocks were crushed and sieved and inclusion-free phengite grains were hand-picked under a binocular microscope. Selected phengites were washed with deionized water in an ultrasonic bath, wrapped in Al-foil, and loaded in Al-irradiation disks with the sanidine from Fish Canyon rhyolite (FC-2, age of 28.02 Ma; Renne

et al., 1998). CaF_2 was also irradiated for correction of reactor-induced interferences on Ca in the USGS TRIGA reactor located at the Denver Federal Center, USA.

Phengite grains of 300–425 μm in size were dated by single-grain total fusion and grains of 250–300 μm were dated by multiple-grain incremental heating. A 50-W Synrad CO_2 laser source was used to heat the samples. The apparent ages in this study (weighted means and plateau averages) are quoted with their standard deviation. Data were reduced by Excel workbooks and corrected for blank level, mass discrimination, interfering Ar isotopes, and decay of ^{37}Ar and ^{39}Ar since time of irradiations. Isoplot (Ludwig, 2003) was used with the resulting isotopic data to calculate plateau and weighted mean ages. Plateaus in this study were defined with at least three or more contiguous increments containing more than 50% percent of the total $^{39}\text{K}_{\text{Ar}}$, with no resolvable slope among ages.

3.4. U-Pb dating

Zircon crystals were separated and embedded in epoxy resin and polished to expose sections through their centers. Cathodoluminescence (CL) and back-scattered images were collected prior to zircon analyses to identify inherited cores, cracks, and inclusions at the University of Belgrade using a JSM-259 6610 LV scanning electron microscope. U-Pb isotope analyses of particular zircon zones used a New Wave Research Excimer 193-nm laser-ablation system attached to a PerkinElmer ELAN DRC-e inductively coupled plasma mass spectrometer (LA-ICP-MS) at the Geological Institute of the Bulgarian Academy of Science. The square ablation pit was approximately 35 μm wide and a frequency of 8 Hz was used for these analyses. The measurement procedure included calibration against an external zircon standard (GJ-1; Jackson et al., 2004) at the beginning, middle, and end of each analytical block. This technique allows a suitable correction for instrumental drift along with the minimization of elemental fractionation effects. Raw data were processed using GLITTER4, a data reduction program of the GEMOC, Macquarie University, Australia. Following careful examination of the time-resolved ratios for each analysis, ratios of $^{207}\text{Pb}/^{206}\text{Pb}$, $^{208}\text{Pb}/^{232}\text{Th}$, $^{206}\text{Pb}/^{238}\text{U}$, and $^{207}\text{Pb}/^{235}\text{U}$ were calculated. Optimal signal intervals for the background and ablation data were selected for each sample and automatically matched with the standard zircon analyses. U-Pb Concordia ages were calculated and plotted using Isoplot (Ludwig, 2003). The NIST610 standard was used as external reference material for the trace element measurements. One measuring block consists of 2 NIST 610 standard analyses followed by sample (zircon) analyses and finishes with 2 NIST 610 analyses. The element concentrations were recalculated using SILLS software (Norman et al., 1998). SiO_2 was fixed at 32.8 weight percent, based on the stoichiometry of zircon.

3.5. (U-Th)/He thermochronology

Apatite crystals were selected from microgranodiorite and dated by (U-Th)/He method. Single-crystal aliquots were dated, usually with 3 aliquots per sample. The crystals were selected carefully; only crystals lacking fractures were used, with well-defined completely convex external morphology. Euhedral crystals were preferred. The shape parameters were determined and archived by multiple digital microphotographs. In the case of zircon crystals the proportion of the length of the prismatic and pyramidal zones was also considered in addition to the lengths and widths.

The crystals were wrapped in platinum capsules of ca. 1 \times 1 mm in size. The Pt capsules were heated with an infrared laser. The extracted gas was purified using a SAES Ti-Zr getter at 450 °C. The chemically inert noble gases and a minor amount of other rest gases were then expanded into a Hiden triple-filter quadrupole mass spectrometer equipped with a positive ion counting detector. Crystals were checked for degassing of He by sequential reheating and He measurement. The residual gas was always below 1%.

Following degassing, samples were retrieved from the gas extraction line, spiked with calibrated ^{230}Th and ^{233}U solutions, and dissolved in a 2% HNO_3 + 0.05% HF acid mixture in Savillex Teflon vials. Spiked solutions were analyzed as 1.4 or 2 mL of ~0.5 ppb U-Th solutions by isotope dilution with a PerkinElmer Elan DRC II ICP-MS and an APEX microflow nebulizer. Samarium, Pt, and Ca were determined by external calibration. The oxide formation rate and potential interference of PtAr-U were always monitored, but the effects of these isobaric argides were negligible relative to the signal of actinides.

4. Results

4.1. Sample descriptions

Thin sections of 50 samples were petrographically examined (Figure 5). Polished thin sections of six samples were prepared for electron probe microanalysis (EPMA) to characterize the compositional variation of the minerals and estimate pressure-temperature (P-T) conditions of metamorphism that affected the region.

Samples S-16C and S-16D were selected for $^{40}\text{Ar}/^{39}\text{Ar}$ ages to define the time of metamorphism exposed in the region. The samples, quartz muscovite schists, have lepidoblastic texture and comprise quartz, albite, chlorite, phengitic white mica, and a small quantity of Fe-oxides, and accessory apatite, sphene, and zircon.

A microgranodiorite, sample 12, was selected for zircon U-Pb geochronology and apatite (U-Th)/He thermochronology. The sample displays porphyritic texture and is composed of quartz, K-feldspar, plagioclase, and amphibole phenocrysts that are mostly altered and minor amounts of zircon, apatite, and opaque minerals.

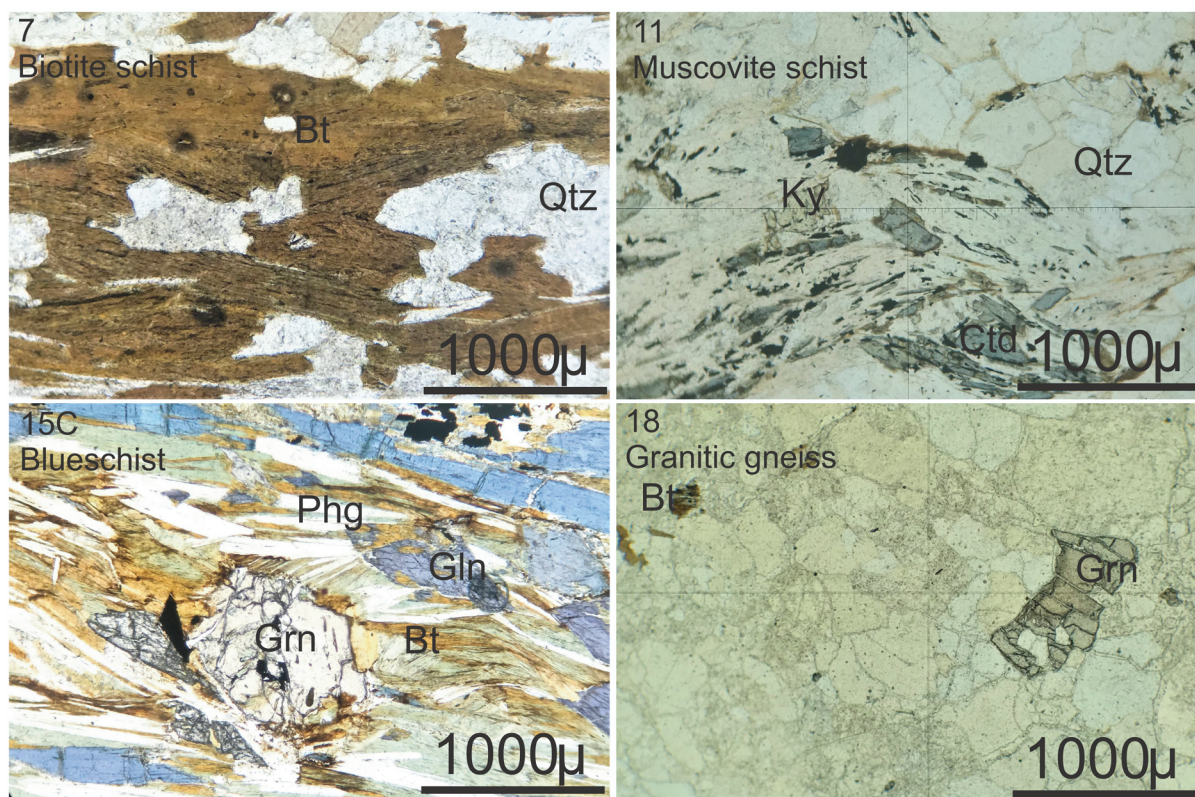


Figure 5. Microphotographs showing mineral paragenesis and textural relations of the metamorphic rocks in the Sivrihisar area of the Tavşanlı Zone (plane polarized light; Qtz: quartz; Bt: biotite; Phg: phengite; Gln: glaucophane; Grn: garnet).

4.2. Mineral chemistry and P-T estimates

The mineral chemistry analyses are given in Tables 1–6. EPMA was done on the albite (Ab), chlorite (Chl), chloritoid (Cld), white mica (Wmca), biotite (Bt), Na-amphibole (Amp), epidote (Ep), and garnet (Grt) minerals from mica schists (7, 11, 23B), metabasite (17B), blueschist (15C), and granite-gneiss (18).

A sample of biotite schist (sample 7) has a lepidogranoblastic texture and is composed of quartz, plagioclase, K-feldspar, white mica, and biotite and minor amounts of apatite, titanite, and zircon as accessory minerals (Figure 5). Chlorite and rare epidote crystals are retrograde phases in the rock. Biotite constitutes as much as 50% of the schist, with a grain size of 1 mm or less, and it is extensively chloritized. Quartz has undulatory extinction, recording effects of late-stage deformation. White micas display Si contents between 2.89 and 2.93 cations on the basis of 11-oxygens (Table 4). X_{Mg} values of biotites are from 0.48 to 0.50 (Table 5).

The muscovite schists studied (samples 11, 23B) have lepidoblastic and granoblastic textures and are composed of quartz, albite, chlorite, chloritoid, white mica, and kyanite and small quantities of hematite, Fe-oxides, and accessory apatite and zircon. Quartz exhibits undulatory

extinction and recrystallization textures indicating late deformation. Prismatic chloritoid and kyanite crystals are of variable size and have elongation subparallel to the main metamorphic foliation. X_{Mg} values of chloritoid in sample 11 are 0.10–0.12 and 0.28–0.3 in sample 23B (Table 3). White micas display Si contents of 3.03–3.17 cations on the basis of 11-oxygens (Table 4).

Blueschist sample 15C has a lepidoblastic texture and comprises albite, white mica, biotite, Na-amphibole (glaucophane), and garnet and small amounts of titanite, epidote, rutile, tourmaline, and Fe-oxides. Sericite and chlorite occur as retrograde phases. Quartz is not common in the blueschist and is observed mainly as inclusions within garnet porphyroblasts. The schistosity is defined by tabular to elongate glaucophane porphyroblasts that have an intense dark blue pleochroism and are commonly microboudinaged. Euhedral titanite crystals are present in the amphibole and white mica matrix. Idioblastic garnet porphyroblasts up to 2 mm in diameter are observed among crystals of white mica and glaucophane. Garnet has the compositional range $Alm_{40-55}Pyp_{3-5}Grs_{17-18}Sps_{22-38}$ and small amounts of TiO_2 (≤ 0.14 wt.%; Table 6). Epidote displays X_{Fe}^3 values of 0.17–0.28 (Table 1). X_{Mg} values of biotites are between 0.49 and 0.50 (Table 5). Na-amphiboles

Table 1. EPMA results of selected Na-amphiboles and epidotes from blueschist and chlorite metabasite.

Rock Sample Mineral	Blueschist 15C Na-Amphibole					Blueschist 15C Epidote			Chlorite metabasite 17B Epidote	
SiO ₂	57.66	57.92	58.32	57.89	58.50	38.43	38.10	38.15	36.72	36.12
TiO ₂						0.06	0.01	0.04	0.05	0.08
Al ₂ O ₃	6.66	6.58	7.55	6.47	7.11	25.75	25.00	25.59	22.18	25.39
FeO	15.37	15.78	15.40	16.41	15.96	13.50	13.84	13.32	13.27	13.48
CaO	1.28	1.54	1.34	1.19	1.39	23.08	21.83	22.42	22.83	22.97
MnO	0.12	0.22	0.19	0.22	0.19	0.21	0.80	0.46	0.17	0.13
MgO	9.80	9.97	9.27	9.47	9.09	0.01				
Na ₂ O	6.17	5.97	5.95	5.87	6.08	0.01	0.01	0.002		
Total	97.06	97.98	98.02	97.49	98.32	100.97	99.50	99.86	97.08	101.95
Si	8.054	8.017	8.059	8.045	8.096	5.848	5.887	5.864	5.963	5.856
Al	1.096	1.073	1.230	1.060	1.160	3.463	3.415	3.477	3.185	3.447
Ti						0.007	0.002	0.005	0.006	0.010
Fe ⁽ⁱⁱ⁾	1.053	0.993	1.118	0.993	1.242					
Fe ⁽ⁱⁱⁱ⁾	0.742	0.834	0.662	0.914	0.605	1.289	1.341	1.284	1.352	1.299
Ca	0.192	0.228	0.198	0.177	0.206	1.881	1.807	1.846	1.986	1.890
Mn	0.014	0.026	0.022	0.026	0.022	0.014	0.053	0.030	0.012	0.009
Mg	2.041	2.057	1.910	1.962	1.875	0.002				
Na	1.671	1.602	1.594	1.582	1.631	0.001	0.001	0.002		
Total	14.862	14.830	14.792	14.759	14.837					
Mg/(Mg+Fe ²)	0.66	0.67	0.63	0.66	0.60					
Al/(Al+Fe ³)	0.60	0.51	0.65	0.53	0.65					
Fe ³ /(Fe ³ +Al ⁶)	0.39	0.43	0.34	0.45	0.33					
Na _B	1.671	1.602	1.594	1.582	1.631					
X _{Fe}						0.274	0.278	0.175	0.297	0.273

Cation occupations on the basis of 23 oxygens for amphiboles and 12.5 oxygens for epidotes.

are characterized by glaucophane composition with X_{Mg} of 0.63–0.68 (Table 1; Figure 6a).

The granite-gneiss sample 18 is a leucocratic, medium-grained strongly deformed rock containing quartz, plagioclase, K-feldspar, microcline, muscovite, and a few biotite and garnet grains. Magnetite, apatite, titanite, zircon, and sericite are accessory minerals. The compositional range of garnets is Alm₅₅₋₅₈Pyp₄₋₅Grs₁₋₈Sps₂₉₋₃₈ (Table 6). Biotites have X_{Mg} values between 0.59 and 0.62 (Table 6). White micas display Si contents between 2.85 and 2.91 cations on the basis of 11-oxygens (Table 4; Figure 6b).

The blueschist sample 15C and granite-gneiss sample 18 were selected for further thermobarometry study. Blueschist and granite gneiss contain different mineral assemblages. Therefore, P-T estimates are approximate. The garnet-biotite Fe-Mg exchange geothermometer has

been widely used for estimating T of metamorphic rocks. The landmark experimental calibrations of Ferry and Spear (1978) and Perchuk and Lavrenteva (1983) form the basis for this geothermometer, together with recent modifications that account for nonideality in the garnet and biotite (e.g., Ganguly and Saxena, 1984; Bhattacharya et al., 1992). We used garnet-biotite thermometry to constrain the metamorphic temperature for both samples (Bhattacharya et al., 1992). We applied six different calibrations published in the literature (Thompson, 1976; Holdaway and Lee, 1977; Ferry and Spear, 1978; Hodges and Spear, 1982; Perchuk and Lavrenteva, 1983; Ganguly and Saxena, 1984; Hackler and Wood, 1989). For the granite-gneiss sample (18) estimated temperatures range from 284 to 397 °C for pressures of 2.5 kbar to estimates between 303 and 413 °C for a pressure of 10 kbar (Figure

Table 2. EPMA results of plagioclases from biotite schist and granite-gneiss.

Rock Sample	Biotite schist 7		Granite-gneiss 18		
SiO ₂	62.39	61.93	64.20	64.30	65.91
Al ₂ O ₃	23.01	23.14	21.96	21.22	20.67
FeO	0.05	0.11	-	0.02	-
CaO	3.56	3.90	2.20	1.33	0.89
Na ₂ O	10.02	9.65	10.70	11.12	11.66
K ₂ O	0.20	0.21	0.11	0.09	0.10
Total	99.27	98.96	99.17	98.11	99.25
Si	2.786	2.775	2.853	2.883	2.918
Al	1.211	1.222	1.150	1.122	1.079
Fe ⁽ⁱⁱ⁾	0.002	0.004	-	0.001	-
Ca	0.171	0.187	0.105	0.064	0.043
Na	0.867	0.839	0.922	0.967	1.001
K	0.012	0.012	0.007	0.005	0.006
X _K	0.013	0.014	-	-	-
X _{Na}	0.986	0.985	0.992	0.993	0.994
X _{Ca}	0.162	0.180	0.101	0.061	0.040

Cation occupations on the basis of 8 oxygens for plagioclase.

Table 3. EPMA results of chlorite and chloritoid from muscovite schist and chlorite metabasite.

Mineral	Chlorite				Chloritoid					
	11	17B			11			23B		
SiO ₂	28.18	28.65	27.81	28.17	24.58	24.74	24.48	24.59	24.50	24.82
TiO ₂	0.04	-	0.02	-	0.04	-	0.05	-	-	-
Al ₂ O ₃	22.56	22.14	18.86	19.82	44.88	44.21	44.76	44.69	44.34	45.24
FeO	25.53	14.58	14.33	17.86	23.31	23.44	22.72	17.26	18.47	17.39
CaO	0.24	0.02	-	0.11	-	-	-	-	-	-
MnO	0.20	0.29	0.34	0.33	0.30	0.33	0.56	3.91	3.93	3.58
MgO	4.9	21.10	23.40	26.55	1.63	1.66	1.75	4.72	4.19	4.69
Na ₂ O	0.11	-	-	-	0.01	0.02	-	-	0.02	-
K ₂ O	1.76	-	-	-	-	-	-	-	-	-
Total	82.87	86.13	864.11	92.19	97.16	96.79	96.71	96.99	97.42	97.59
Tetrahedral										
Si	3.116	2.758	2.860	2.696	1.841	1.861	1.841	1.844	1.837	1.846
Al ^(iv)	2.940	2.6043	2.286	2.235	4.214	4.173	4.215	4.134	4.115	4.150
Octahedral										
Al ^(vi)	-	-								
Ti	0.003	-	0.002	-	0.002	-	0.003	-	-	-
Fe ⁽ⁱⁱ⁾	2.361	1.216	1.232	1.429	1.460	1.475	1.429	-	-	-
Fe ⁽ⁱⁱⁱ⁾	-	-	-	-	1.841	1.861	1.841	1.844	1.837	1.846
Ca	0.028	0.002	-	0.011	-	-	-	-	-	-
Mn	0.019	0.024	0.030	0.027	0.019	0.021	0.036	0.249	0.250	0.001
Mg	0.808	3.138	3.587	3.788	0.183	0.180	0.197	0.528	0.468	0.520

Cation occupations on the basis of 14 oxygens for chlorites, 12 oxygens for chloritoids.

Table 4. EPMA results of white micas from muscovite schist, biotite schist, blueschist, and granite-gneiss.

Rock	Biotite schist			Muscovite schist			Blueschist			Granite-gneiss			Muscovite schist		
Sample	7			11			15C			18			23B		
SiO ₂	44.68	44.60	46.25	48.88	49.17	48.39	53.51	54.34	53.13	46.49	45.32	46.14	46.56	47.24	48.36
TiO ₂	0.62	0.90	0.62	0.08	0.08	0.06	0.05	0.11	0.12	0.03	0.34	0.24	0.12	0.07	0.09
Al ₂ O ₃	39.46	39.46	40.14	34.75	34.71	39.38	25.15	25.11	26.55	36.73	34.93	34.90	34.41	34.27	34.76
FeO	1.11	1.10	0.88	3.21	3.58	1.65	4.35	4.80	4.68	3.12	5.58	4.75	3.48	3.62	3.87
CaO	0.04	-	0.01	0.02	0.01	0.06	-	-	-	0.01	-	0.06	0.04	0.01	0.02
MnO	0.71	0.04	0.03	-	0.01	-	0.01	0.02	-	0.12	0.23	0.14	0.05	-	-
MgO	-	0.71	0.68	0.96	1.09	0.44	4.19	4.16	3.55	0.51	1.28	1.20	1.04	1.14	1.19
Na ₂ O	0.58	0.58	0.52	0.47	0.63	3.40	0.01	0.04	0.10	0.09	0.23	0.27	0.49	0.39	0.47
K ₂ O	10.36	10.36	10.61	8.75	9.25	5.45	10.02	11.02	10.65	9.96	10.38	10.50	9.61	9.73	9.79
Total	97.56	97.12	99.13	96.49	97.92	98.22	96.65	98.99	98.13	96.46	97.67	97.58	95.18	95.848	97.94
Tetrahedral Si	2.904	2.894	2.933	3.172	3.163	3.035	3.507	3.505	3.449	3.045	2.993	3.034	3.098	3.121	3.128
Al	1.096	1.106	1.067	0.828	0.838	0.965	0.493	0.495	0.551	0.955	1.007	0.966	0.902	0.879	0.872
Octahedral															
Ti	0.031	0.044	0.030	0.004	0.004	0.003	0.003	0.259	0.006	0.002	0.017	0.012	0.006	0.004	0.004
Al	1.926	1.912	1.933	1.830	1.795	1.946	1.449	1.413	1.480	1.881	1.712	1.739	1.796	1.789	1.778
Fe ⁽ⁱⁱ⁾	0.060	0.060	0.047	0.174	0.193	0.087	0.239	0.005	0.254	0.171	0.308	0.261	0.194	0.200	0.210
Mg	-	0.069	0.064	0.093	0.105	0.042	0.410	0.401	0.344	0.050	0.127	0.118	0.104	0.113	0.116
Interlayer															
Ca	0.003	-	0.001	0.001	0.001	0.004	-	-	-	0.001	-	0.004	0.003	0.001	0.001
Mn	0.002	0.002	0.002	-	0.001	-	0.001	0.002	0.001	0.007	0.013	0.008	0.003	-	-
Na	0.073	0.073	0.065	0.059	0.079	0.413	0.002	0.006	0.014	0.012	-	0.035	0.064	0.050	0.060
K	0.859	0.858	0.858	0.725	0.759	0.437	0.838	0.907	0.882	0.833	0.875	0.881	0.816	0.820	0.808

Cation occupations on the basis of 11 oxygens for white micas.

7a). Considering that the mineral paragenesis and Si contents of white mica are 2.9–3.1 per formula unit, we consider the maximum pressure experienced by this sample to be below 5 kbar.

The same six different calibrations mentioned above for sample 18 were used for estimation of thermometry of sample 15C. Temperatures of 335–458 °C are obtained for 2.5 kbar and 340–484 °C for 10 kbar (Figure 7b). Considering the presence of glaucophane and high Si values of the phengitic white micas (with 3.4–3.5 cations per formula unit), pressures that affected the sample are considered to be higher than 10 kbar (see also discussions of phengite compositions as a function of pressure by Parra et al., 2002). Estimates of ca. 15 kb for the maximum pressures experienced by similar rocks examined in the NW part of the present study area (Whitney et al., 2011) are also consistent with our estimation.

4.3. Geochemistry

4.3.1. Metasedimentary rocks

Seventeen samples were selected for major and trace element analysis and the results are given in Table 7. They have high contents of SiO₂, whereas Na₂O contents vary from 0.09 to 2.45 wt.% and K₂O ranges up to 4.90 wt.%. Chondrite-normalized REE patterns of the samples exhibit regular, smooth patterns, consistent with the REE remaining immobile during the blueschist-facies metamorphism (Figure 8a). LREE enrichment shows as much felsic igneous rock as mafic rock within a source area (Taylor and McLennan, 1985). The presence of a weak negative Eu anomaly suggests that the source area included ancient continental crust or volcanic arc rocks (McLennan et al., 1995; Silaupa, 2002; Asiedu et al., 2004). The chondrite-normalized REE patterns are similar with little diversity for sediments associated with active continental

Table 5. EPMA results of biotite from biotite schist, blueschist, and granite-gneisses.

Rock Sample	Biotite schist 7			Blueschist 15C			Granite-gneiss 18		
SiO ₂	36.11	36.55	36.78	35.67	37.45	36.66	36.77	37.28	37.01
TiO ₂	2.66	2.61	2.22	2.10	2.46	2.33	0.56	0.02	0.14
Al ₂ O ₃	20.64	21.61	21.62	17.70	17.89	17.41	20.32	17.88	19.02
FeO	17.63	17.38	17.71	18.06	18.01	18.45	15.80	16.01	16.10
CaO	-	0.01	0.01	0.02	0.01	0.01	-	0.01	-
MnO	0.25	0.26	0.27	0.33	0.32	0.29	0.01	0.02	0.01
MgO	9.96	9.32	9.86	10.02	10.41	10.34	13.13	14.69	14.20
Na ₂ O	0.11	0.14	0.13	0.14	0.13	0.12	0.39	0.38	0.29
K ₂ O	9.74	9.67	9.92	9.45	9.67	9.71	8.79	8.81	8.89
Total	96.50	96.95	97.91	93.49	96.34	95.32	95.77	95.10	95.66
Si	2.668	2.676	2.673	2.757	2.795	2.781	2.810	2.780	2.742
Ti	0.148	0.144	0.121	0.122	0.138	0.138	0.032	0.001	0.008
Al	1.798	1.865	1.852	1.613	1.574	1.557	1.568	1.572	1.662
Fe ⁽ⁱⁱ⁾	1.090	1.064	1.076	1.168	1.124	1.170	1.010	0.998	0.998
Ca	-	0.001	0.001	0.002	0.001	0.001	-	0.001	-
Mn	0.016	0.016	0.017	0.022	0.020	0.019	0.001	0.001	-
Mg	1.097	1.018	1.069	1.154	1.158	1.169	1.495	1.633	1.568
Na	0.017	0.021	0.019	0.021	0.019	0.018	0.058	0.055	0.042
K	0.918	0.903	0.920	0.932	0.921	0.940	0.857	0.838	0.840
X _K	0.981	0.977	0.979	0.978	0.980	0.981	0.937	0.938	0.952
X _{Na}	0.018	0.022	0.020	0.022	0.020	0.019	0.063	0.062	0.048
X _{Mg}	0.501	0.488	0.498	0.497	0.507	0.499	0.596	0.620	0.611

Cation occupations on the basis of 11 oxygens for biotites.

margin settings, which are explained by different tectonic settings (Bhatia and Crook, 1986).

The significance of the concentrations of some elements (e.g., Na, K, Rb, and Sr) are limited because they are mobile during metamorphism and deformations (Bebout, 2007; Volkova et al., 2009) while others (e.g., Ti, Zr, Hf, Nb, Sc, Cr, Ni, V, Co, Th) and the REEs are immobile and can be used for determinations of sediment provenance, magmatic evolution, and tectonic setting (Taylor and McLennan, 1985; Bhatia and Crook, 1986). Sedimentary sources are commonly assigned to different tectonic settings based on immobile element chemical compositions (Bhatia, 1983; Bhatia and Crook, 1986). The metasedimentary samples plot in the magmatic arc-related field on the La–Th–Sc diagram of Girty and Barber (1993; Figure 8b).

4.3.2. Metabasites

The chemical compositions of the metabasites are given in Table 7. They contain highly variable amounts of SiO₂ (25.1%–83.90%) and Al₂O₃ (1.52%–16.25%);

high concentrations of TiO₂ (up to 4.66%), Fe₂O₃ (up to 15.40%), MgO (up to 35.10%), and CaO (up to 5.01%); and low concentrations of Na₂O+K₂O (less than 0.09%). The metabasitic sample (17E) with high SiO₂ content was over-silicified. These rocks are also strongly enriched with ferromagnesian trace elements (Co, 110.5 ppm; Cr, 4840 ppm; Ni, 2320 ppm) and other highly incompatible elements. These geochemical and mineralogical results suggest that these rocks formed in the midoceanic plate boundary. These samples are characterized by high REE concentrations, but generally have low Eu anomalies and strong Nb–Ta enrichments (Figures 9a and 9b).

4.4. Phengite ⁴⁰Ar/³⁹Ar Ages

Phengitic muscovite crystals (with more than 3 Si per formula unit) were separated and dated from two quartz muscovite schist samples (S-16C and S-16D). ⁴⁰Ar/³⁹Ar data were obtained by laser-controlled incremental heating and also in separate experiments with fusion of single crystals (Figure 10; see also Tables 8 and 9). A single muscovite

Table 6. EPMA results of garnets from blueschist and granite-gneiss.

Rock Sample	Blueschist 15C			Granite-gneiss 18		
	SiO ₂	37.20	37.14	37.12	35.70	36.19
TiO ₂	0.02	0.12	0.14	0.18	0.42	0.12
Al ₂ O ₃	21.11	20.86	20.62	20.89	20.54	21.03
FeO	24.47	20.09	17.63	24.47	26.32	24.37
CaO	5.97	6.04	6.10	0.65	2.75	0.72
MnO	9.58	14.20	16.50	15.70	13.09	16.54
MgO	1.14	0.91	0.83	1.04	1.18	1.05
Total	99.53	99.40	98.97	98.66	100.53	100.07
Si	12.029	12.044	12.085	5.924	5.902	5.930
Al ^(iv)	-	-	-	-	-	-
Al	6.034	5.980	5.935	4.085	3.949	4.060
Ti	0.005	0.032	0.037	0.024	0.052	0.016
Fe ⁽ⁱⁱ⁾	3.308	2.723	2.400	3.396	3.590	3.338
Fe ⁽ⁱⁱⁱ⁾	-	-	-	-	-	-
Ca	1.035	1.050	1.064	0.116	0.482	0.127
Mn	1.312	1.951	2.276	2.207	1.809	2.294
Mg	0.276	0.222	0.203	0.260	0.289	0.258
X _{Mg}	-	-	-	0.071	0.075	0.071
Fe/Fe+Mg	0.922	0.924	0.922	0.928	0.925	0.928
Py	4.659	3.728	3.416	4.343	4.681	4.289
Alm	55.770	45.807	40.392	56.802	58.189	55.469
Gro	17.446	17.655	17.902	1.937	7.806	2.110
Sp	22.124	32.811	38.290	36.918	29.323	38.132

Cation occupations on the basis of 24 oxygens for garnets.

porphyroblast from sample 16C defines a plateau age of 82.50 ± 0.18 Ma (MSWD = 0.75, probability = 0.75, all age data are quoted with the standard deviation, and plateau or statistical mean ages include the error in estimating the J-value, 0.125%), with 99% of the ³⁹Ar_K released (Figure 10). Sample 16D contains smaller muscovite crystals, and incremental heating of an aliquot of 20 crystals from this sample yielded a plateau age of 83.48 ± 0.14 Ma (MSWD = 1.10, probability = 0.36), with 98% of the ³⁹Ar_K released (Figure 10). Fusion of single crystals yielded mean ages (Figure 10) that are statistically identical to the respective plateau ages obtained by incremental heating (though the results for samples 16C and 16D differ consistently by ca. 1 Ma, and the ages for single crystals of sample 16D are more variable). The consistencies of ages for the multiple-grain and single-crystal analytical techniques are taken as evidence that these phengitic muscovite samples are not substantially affected by unsupported, extraneous ‘excess’

⁴⁰Ar, as is common in ⁴⁰Ar/³⁹Ar studies of phengite (see discussions of Warren et al., 2011). The ⁴⁰Ar/³⁹Ar ages for these samples are interpreted to record retention of radiogenic ⁴⁰Ar as produced by decay of potassium in these muscovite crystals, beginning at ca. 83 Ma.

4.5. Zircon U-Pb geochronology and mineral chemistry

Thirty-eight spot analyses of distinct zircon zones of 30 grains were made from a hypabyssal rock (sample 12). The zircons studied are medium to long prismatic (Figure 11). They reveal well-expressed oscillatory zonation. Some of the zones have endured magmatic corrosion. Some of the crystals show metamictization and recrystallization and this probably lead to Pb-loss and discordance in some of the analyses. The average age of laser spots placed in the oscillatory zones is 50.52 ± 0.33 Ma (Figure 12a).

The crystal analyses are typical for the magmatic-grown zircons’ Th/U ratio (between 0.4 and 0.64) and chondrite normalized pattern with Ce maximum; Pr, Nd,

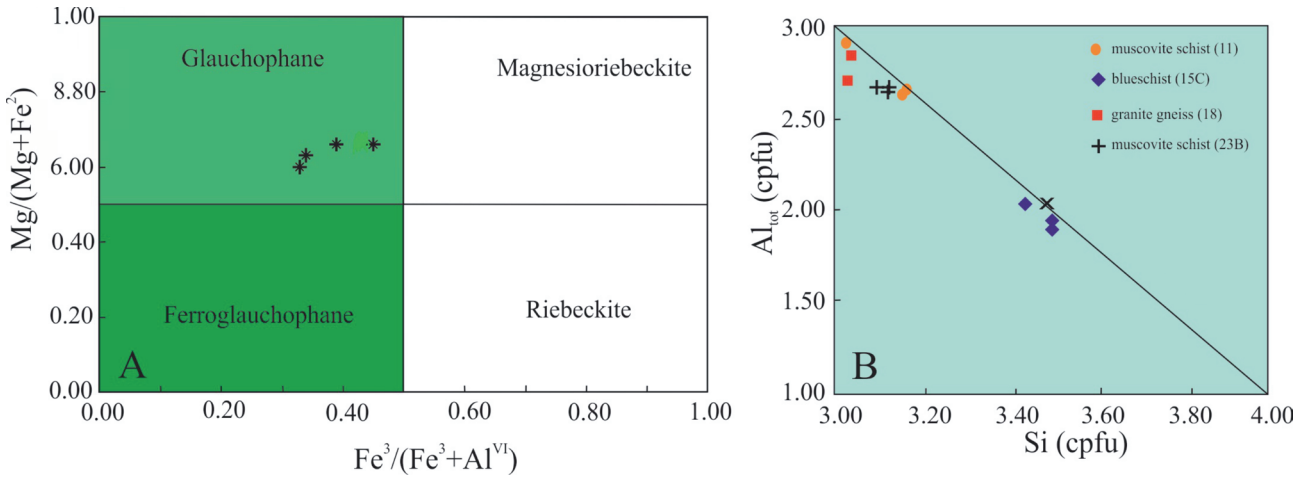


Figure 6. a) Fe³/(Fe³+Al^{VI}) versus Mg/(Fe² + Mg) diagram of amphibole. The dividing lines were adopted from Leake et al. (1997). b) Variation of Al_{tot} versus Si in white micas from the studied samples of the Tavşanlı Zone.

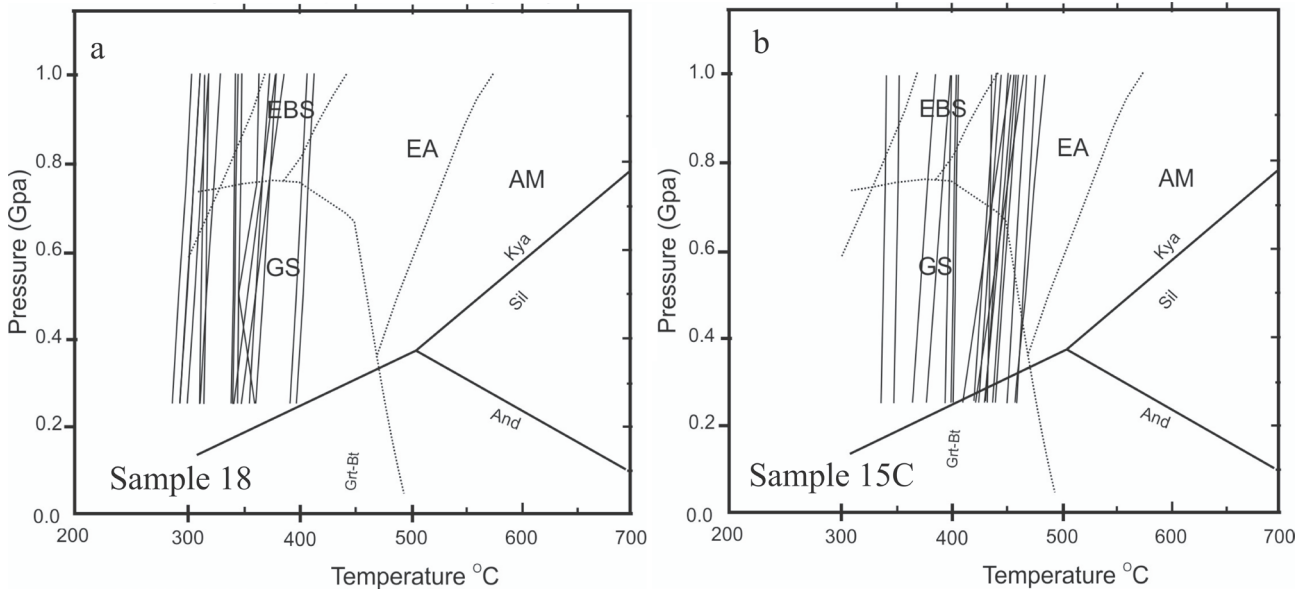


Figure 7. Combination of individual P-T estimates deduced for the basement unit from samples 18 (a) and 15C (b). Garnet-biotite transition according to Bhattacharya et al. (1992). Approximate boundaries between metamorphic facies are shown as dotted lines: GS – greenschist facies; EBS – epidote blueschist facies; EA – epidote–amphibolite facies; AM – amphibolite facies (Krogh et al., 1994 and references therein).

and Eu minimum; and high abundance of HREEs over LREEs (Figure 12a). One of the zircon crystals (grain 37) contains a core with magmatic resorption, and the newly grown zone contains higher U, Th, and REE concentrations (Figure 12b). This zone probably crystallized during the final magmatic stages and accommodated most of the U, Th, and REEs left in the magma. The Ti-in-zircon geothermometer (Claiborne et al., 2010) shows values in the range of 790–830 °C (Table 10).

4.6. Thermochronological results

We report here new apatite (U-Th)/He cooling ages from the TZ. The average AHe ages corrected for alpha ejection range from 41.9 to 34.4 Ma with an average of 38.5 Ma (Table 11).

5. Discussion

In order to constrain the time of metamorphism in the TZ, we present new high-precision ⁴⁰Ar/³⁹Ar ages for phengites

Table 7. Major and trace element compositions of metamorphic rocks from the Tavşanlı Zone.

	5A	5B	7	13	13A	15A	15B	15D	15E	15F	16A	16B	16C	16D	16E	16F	15C	17A	17B	17C	17D	17E
SiO ₂	92.4	93.2	58.1	42.7	50.9	23.8	41.2	90.7	89.6	91.4	84.2	44.8	77.0	79.1	70.9	92.5	46.9	27.9	27.7	25.1	41.2	83.9
Al ₂ O ₃	2.38	2.57	16.85	6.67	16.0	3.57	10.15	3.09	3.73	2.86	5.50	8.21	2.33	7.39	6.11	2.79	13.55	15.5	16.25	12.85	1.52	2.78
Fe ₂ O ₃	2.19	1.76	6.85	3.17	9.44	1.98	7.12	2.71	3.22	2.58	3.12	8.92	1.94	3.90	3.69	2.53	12.65	15.4	14.1	16.7	8.52	2.12
MgO	0.38	0.25	3.56	1.86	7.60	1.12	6.70	0.49	0.79	0.59	1.56	13.4	4.00	1.86	2.02	0.45	8.28	23.8	20.7	24.8	35.1	0.36
CaO	0.23	0.21	1.07	25.2	10.2	38.4	14.45	0.47	0.48	0.72	1.28	9.69	7.86	0.46	7.72	0.2	1.37	2.62	4.28	2.82	0.13	5.01
Na ₂ O	0.19	0.50	2.40	2.05	2.45	0.05	0.53	0.26	0.56	0.11	0.16	0.60	0.09	1.32	0.12	0.04	1.62	0.01	0.01	0.01	0.01	0.06
K ₂ O	0.76	0.86	4.90	0.13	0.23	1.06	1.26	1.06	1.12	1.13	1.79	0.03	0.68	2.09	1.27	0.97	4.48	0.02	0.01	0.01	0.01	0.09
TiO ₂	0.11	0.08	0.92	0.33	0.77	0.22	1.59	0.13	0.17	0.12	0.24	1.52	0.10	0.34	0.5	0.13	0.69	2.59	4.14	4.66	0.11	0.13
P ₂ O ₅	0.10	0.11	0.07	0.12	0.06	0.06	0.41	0.09	0.10	0.08	0.05	0.24	0.07	0.07	0.17	0.13	0.04	0.76	0.97	1.82	0.05	0.09
MnO	0.29	0.21	0.13	0.25	0.21	0.07	0.14	0.21	0.30	0.45	0.19	22.0	0.22	0.31	0.59	0.29	0.37	0.20	0.20	0.19	0.08	0.25
LOI	0.76	0.38	3.39	18.8	3.81	30.9	13.35	0.77	1.07	1.02	2.78	11.8	7.16	2.00	7.82	0.46	5.74	10.15	9.65	9.88	11.7	4.61
Ba	163.5	148.5	719	27.0	39.7	141.5	168.5	279	209	201	303	7.3	74.6	299	333	404	641	6.7	3.5	6.4	4.1	295
Ce	17.3	11.9	82.9	36.7	6.3	24.8	47.8	21	20.6	21.2	51.9	41.7	24.2	53.6	40.5	19.2	4.3	321	180.5	254	7.2	29.30
Co	9.7	7.2	18.6	16.8	45.0	7.7	20.6	14.4	22.8	16.9	20.2	65.0	12.0	25.3	26.8	12.9	72.3	63.3	60.5	63.7	110.5	18.4
Cr	40	30	110	50	290	30	170	20	40	20	40	1110	20	60	100	20	440	390	150	150	4840	30
Cs	1.98	1.14	9.05	0.05	0.2	1.04	1.36	1.51	2.18	2.48	3.74	0.09	0.85	3.87	1.33	1.89	7.57	0.02	0.02	0.02	0.03	1.34
Cu	42	10	9	39	38	29	35	26	66	18	23	56	29	29	77	20	1060	79	17	68	7	14
Dy	1.86	1.69	4.91	3.01	3.32	1.99	4.32	1.57	1.83	1.85	2.84	3.57	2.29	3.07	3.48	2.13	1.84	16.4	8.55	7.64	0.44	2.97
Er	1.14	1.10	2.70	1.49	2.27	1.09	2.15	0.79	1.10	1.13	1.59	1.84	1.12	1.79	2.02	1.3	1.17	7.44	4.28	3.02	0.23	1.44
Eu	0.52	0.32	1.36	0.94	0.73	0.57	1.50	0.51	0.44	0.47	0.73	1.38	0.63	0.80	0.94	0.5	0.26	7.5	5.70	3.95	0.15	0.84
Ga	3.8	4.20	271	6.10	15.10	4.60	13.30	4.20	4.70	4.10	7.60	11.8	3.30	9.40	8	4.1	14.90	13.7	13.70	7.40	2.20	3.5
Gd	2.21	1.61	5.86	3.71	2.72	2.37	5.31	2.22	1.91	2.05	3.23	4.39	2.82	3.43	3.79	2.37	1.27	20.7	11.85	12.90	0.56	3.67
Hf	0.80	0.60	6.70	1.10	1.30	1.10	4.10	0.80	1.00	0.80	1.50	3.10	0.70	1.90	1.7	0.8	1.20	16.9	9.50	14.1	0.70	0.9

Table 7. (Continued).

Ho	0.41	0.39	0.97	0.58	0.75	0.39	0.83	0.29	0.40	0.40	0.57	0.70	0.43	0.63	0.72	0.47	0.40	2.98	1.62	1.31	0.08	0.57
La	11.7	8.6	42.7	19.1	2.8	15.7	26.8	11.6	10.1	10.7	16.2	24.5	12.6	19.4	20.7	10.7	2.5	194.5	113.0	144.0	4.1	17.2
Lu	0.18	0.17	0.41	0.17	0.33	0.13	0.27	0.11	0.14	0.15	0.21	0.22	0.13	0.23	0.27	0.18	0.16	0.91	0.51	0.36	0.03	0.16
Nb	3.10	3.70	15.9	3.80	1.70	6.60	31.00	2.70	3.50	2.80	5.70	29.8	2.30	7.20	9.3	3.2	3.60	125	177	70.6	3.30	3.30
Nd	11.6	7.60	37.7	19.6	5.50	13.60	26.50	11.7	9.80	10.0	15.2	20.8	13.4	17.0	18.3	9.6	3.20	122.5	75.0	113.00	3.30	18.00
Ni	30	22	56	42	108	23	88	23	33	26	49	791	34	66	72	31	144	335	148	224	2320	50
Pr	2.88	1.93	9.88	4.81	1.03	3.35	6.50	2.83	2.42	2.50	3.90	5.32	3.31	4.43	4.65	2.42	0.69	34.70	19.90	29.70	0.84	4.36
Rb	27.2	27.8	222	2.10	4.3	28.30	34	34.5	38.7	38.8	72.2	0.6	22	70.2	33.2	37.6	140	0.3	0.20	0.20	0.20	32.5
Sm	2.26	1.60	7.14	4.23	1.86	2.76	5.75	2.39	1.96	2.04	3.38	4.35	2.99	3.57	3.74	2.09	0.98	24.1	13.45	17.45	0.58	3.77
Sn	1	1	3	1	1	1	2	1	2	1	2	2	1	2	2	1	1	5	4	1	1	1
Sr	44.2	31	129	189	135	862	291	33.9	16.6	16.4	11	243	132	46.7	84.6	19.3	44.6	34.4	53.6	85.1	5.9	19.3
Ta	0.2	0.2	1	0.3	0.1	0.4	1.9	0.2	0.2	0.2	0.4	1.7	0.1	0.5	0.6	0.2	0.1	23.2	7.70	5.00	0.30	0.20
Tb	0.32	0.27	0.87	0.53	0.50	0.34	0.78	0.30	0.30	0.31	0.51	0.65	0.40	0.53	0.6	0.35	0.27	3.12	1.62	1.59	0.08	0.53
Th	2.44	2.10	12.4	3.98	0.30	2.84	4.98	2.93	2.69	2.70	5.31	3.60	2.29	6.86	4.84	2.59	15C	32.0	16.1	13.05	0.49	3.09
Tl	0.50	0.50	1.10	0.50	0.5	0.50	0.50	0.50	0.50	0.50	0.60	0.50	0.50	0.90	0.50	0.50	46.9	0.5	0.5	0.5	0.5	0.5
Tm	0.18	0.19	0.41	0.20	0.32	0.16	0.30	0.12	0.17	0.17	0.24	0.25	0.14	0.26	0.30	0.20	13.55	1.06	0.59	0.38	0.20	
U	1.88	1.25	3.25	0.90	13A	0.57	1.69	0.21	0.88	0.85	0.55	0.81	0.30	1.25	0.86	0.09	12.65	2.32	1.64	1.27	0.30	0.48
V	15	9	110	52	50.9	66	158	8	26	10	51	145	9	56	89	21	8.28	264	243	153	5	71
W	3	1	2	1	16.0	1	1	1	1	1	2	1	1	2	1	1	1.37	1	1	5	1	8
Y	13.8	13.2	28.4	18.8	9.44	13.00	24.20	8.80	11.9	11.6	15.9	20.0	11.9	17.4	22.5	13.5	1.62	76.4	46.8	32.1	2.00	16.3
Yb	1.04	1.11	2.54	1.22	7.60	0.91	1.90	0.70	0.98	1.06	1.53	1.54	0.93	1.62	1.94	1.17	4.48	6.75	3.55	2.32	0.19	1.20
Zn	46	26	109	45	10.2	41	101	37	53	31	57	102	42	63	75	30	0.06	183	225	135	35	53
Zr	30	20	250	40	2.45	40	170	30	40	30	60	130	30	70	70	30	0.69	790	440	600	30	30
Total	100	100	98	101	100	101	97	100	101	101	101	99	101	99	101	100	0.37	99	98	98	99	100

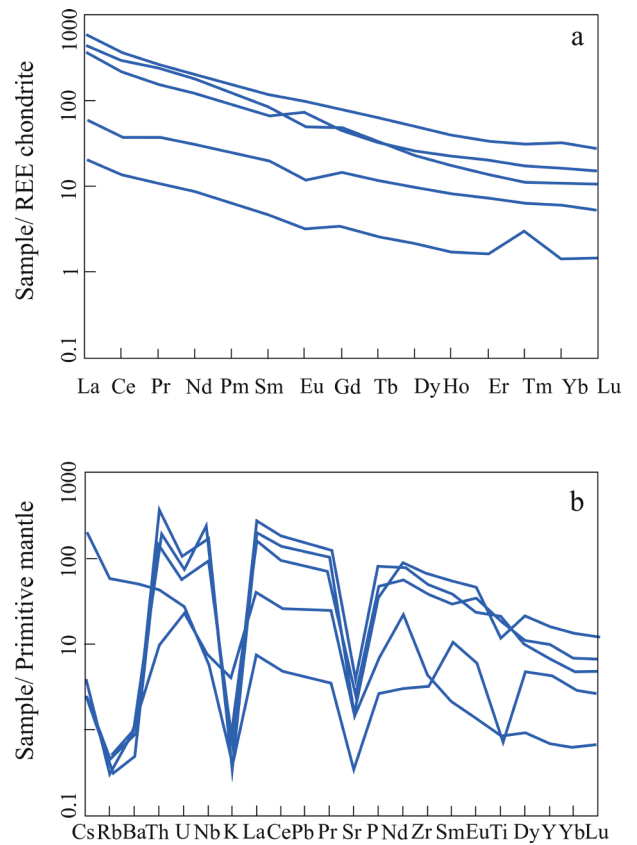
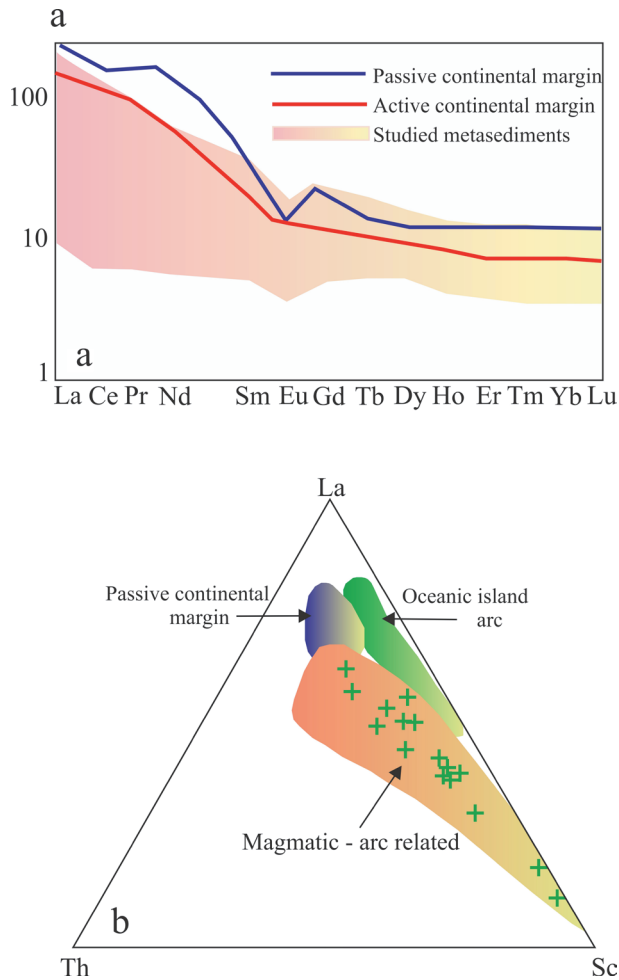


Figure 9. a) Chondrite-normalized diagram of the metapelites (normalizing values from Boynton, 1984). b) Primitive mantle-normalized diagram of the metapelites (normalizing values from Sun and McDonough, 1989).

Figure 8. a) Spider diagrams of the metapelites (normalizing values from Taylor and McLennan, 1985). b) Tectonic discrimination diagram of the studied metasediments (Girty and Barber, 1993).

in two quartz muscovite schists (16C and 16D) representing greenschist facies that yielded multigrain plateau ages and means for single crystals (fused) of 82.5 from the Sivrihisar region of the TZ. $^{40}\text{Ar}/^{39}\text{Ar}$ ages were obtained by a combination of laser-controlled incremental heating and single-crystal fusion methods. The metamorphism that affected the region has been studied several researchers (Sherlock et al., 1999; Candan et al., 2005; Seaton et al., 2009; Özdamar et al., 2012; Pourtaeu et al., 2013). The timing of HP/LT metamorphic events is still debated, because geochronological studies of the blueschists of the TZ have yielded a wide range of ages (60–192 Ma), its eclogite metamorphics have yielded 83 Ma, and the timing of metamorphism has not been well studied. Therefore, the measured $^{40}\text{Ar}/^{39}\text{Ar}$ age could provide useful information about the history of the greenschist facies metamorphism

of the TZ. White mica $^{40}\text{Ar}/^{39}\text{Ar}$ ages have been widely used to determine the timing of metamorphism in exhumed subduction complexes (Sherlock et al., 1999; Agard et al., 2002; Federico et al., 2005). This method is well suited to dating HP/LT rocks because of the relatively low temperatures (<600 °C) of peak metamorphism and white mica may grow or recrystallize during prograde, peak, and/or retrograde parts of the pressure–temperature path. An important question in the interpretation of white mica $^{40}\text{Ar}/^{39}\text{Ar}$ ages is whether the ages represent the timing of crystallization or cooling. If the mica crystallized or experienced temperatures above the closure temperature for Ar in white mica (~350–400 °C), then the $^{40}\text{Ar}/^{39}\text{Ar}$ age should represent a cooling age that is younger than the crystallization age of the mica (Wijbrans and McDougall, 1986). Temperature conditions are estimated at 303–484 °C and minimum pressures of 10 kbar for micaschists and associated rocks of the study area in the Sivrihisar region of the TZ and the $^{40}\text{Ar}/^{39}\text{Ar}$ ages generally record closure between about 83.5 and 82.5 Ma (Figure 10).

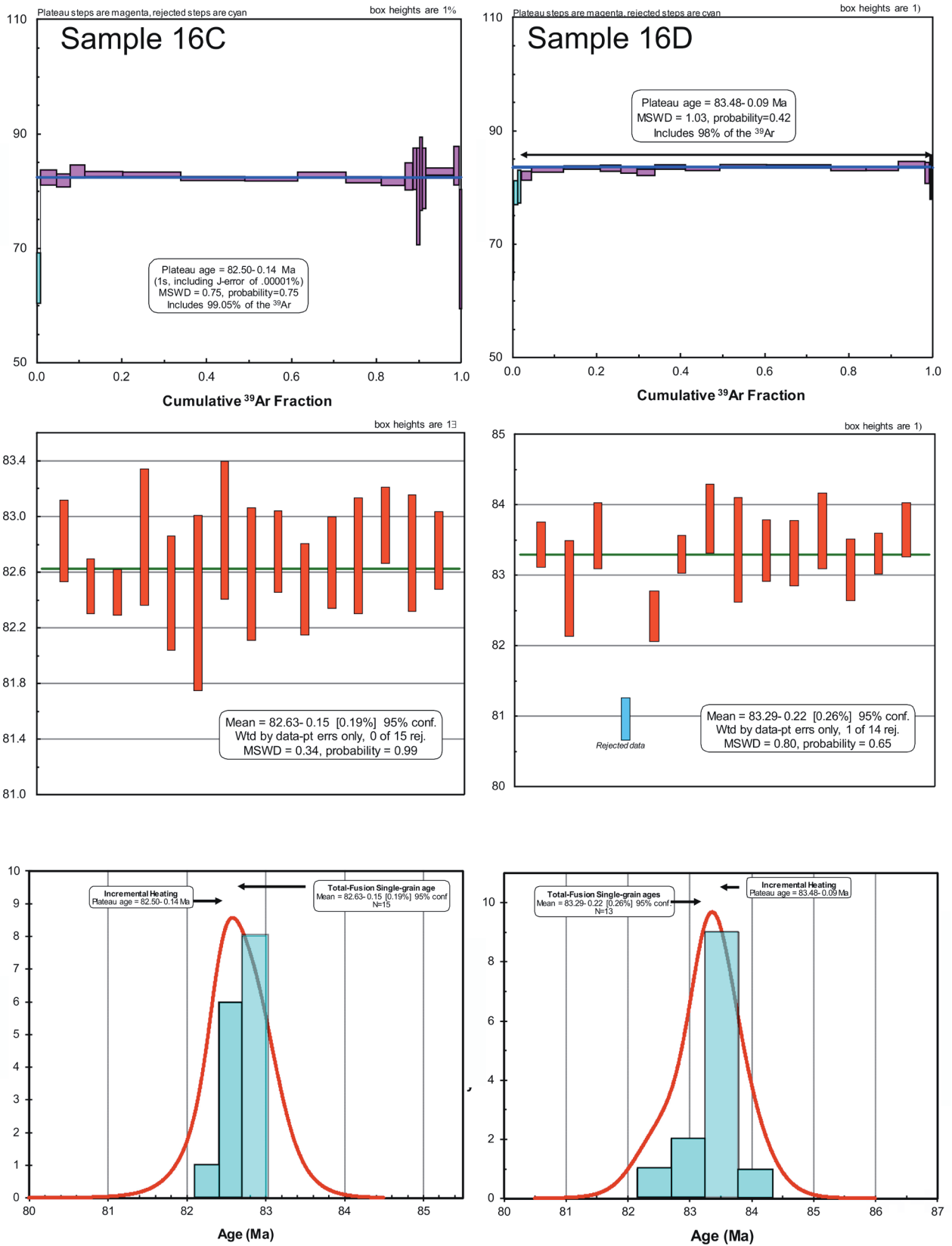


Figure 10. $^{40}\text{Ar}/^{39}\text{Ar}$ ages from the metamorphics (sample 16C left and 16D right).

Table 8. Incremental heating ⁴⁰Ar/³⁹Ar dating of the sample 16C.

Steps	P	t	40 V	39 V	38 V	37 V	36 V	Moles ⁴⁰ Ar*	%Rad	R	Age (Ma)	%-SD				
1	0.4	15	0.009860	±0.000306	±0.000149	0.000030	±0.000035	0.000170	±0.000130	0.000011	±0.000026	6.90E-17	68.11%	11.9429	±181.98	121.03%
2	0.5	15	0.138935	±0.000485	±0.000127	0.000206	±0.000033	0.000252	±0.000194	0.000127	±0.000023	9.73E-16	72.92%	5.0288	±4.35	6.70%
3	0.6	15	0.556137	±0.001198	±0.000453	0.001222	±0.000077	0.000984	±0.000200	0.000108	±0.000025	3.89E-15	94.29%	6.4207	±1.27	1.54%
4	0.6	15	0.464163	±0.000825	±0.000250	0.000838	±0.000041	0.000044	±0.000081	0.000065	±0.000020	3.25E-15	95.84%	6.3836	±1.12	1.37%
5	0.6	15	0.504885	±0.000924	±0.000314	0.000983	±0.000045	0.000081	±0.000160	0.000032	±0.000022	3.54E-15	98.15%	6.5051	±1.14	1.37%
6	0.7	15	1.291286	±0.001688	±0.000416	0.002595	±0.000054	0.000743	±0.000121	0.000050	±0.000022	9.04E-15	98.86%	6.4710	±0.47	0.56%
7	0.7	15	1.973405	±0.002065	±0.000723	0.003911	±0.000073	0.000107	±0.000196	0.000117	±0.000023	1.38E-14	98.25%	6.4662	±0.36	0.44%
8	0.8	15	2.162627	±0.001809	±0.000617	0.004174	±0.000052	0.000609	±0.000236	0.000150	±0.000024	1.51E-14	97.96%	6.4040	±0.33	0.40%
9	0.8	15	1.766145	±0.001291	±0.000568	0.003584	±0.000077	0.000180	±0.000249	0.000169	±0.000018	1.24E-14	97.17%	6.3989	±0.32	0.39%
10	0.8	15	1.627983	±0.001211	±0.000478	0.003329	±0.000052	0.000930	±0.000257	0.000095	±0.000023	1.14E-14	98.27%	6.4551	±0.39	0.48%
11	0.9	15	1.222606	±0.001206	±0.000516	0.002377	±0.000057	0.000603	±0.000194	0.000109	±0.000022	8.56E-15	97.37%	6.3932	±0.51	0.63%
12	0.9	15	0.807702	±0.001535	±0.000510	0.001583	±0.000050	0.000883	±0.000208	0.000098	±0.000020	5.66E-15	96.43%	6.3604	±0.73	0.90%
13	0.9	15	0.271950	±0.000419	±0.000272	0.000421	±0.000059	0.001112	±0.000196	0.000021	±0.000024	1.90E-15	97.73%	6.4263	±2.31	2.80%
14	1.0	15	0.150602	±0.000620	±0.000127	0.000257	±0.000046	0.000224	±0.000184	-0.000005	±0.000021	1.05E-15	101.05%	6.5450	±3.59	4.27%
15	1.0	15	0.071148	±0.000371	±0.000153	0.000021	±0.000035	0.000077	±0.000160	0.000016	±0.000024	4.98E-16	93.37%	6.1576	±8.38	10.60%
16	1.1	15	0.078440	±0.000275	±0.000128	0.000163	±0.000042	0.000626	±0.000216	-0.000008	±0.000020	5.49E-16	102.90%	6.4636	±6.36	7.67%
17	1.2	15	0.128932	±0.000749	±0.000082	0.000176	±0.000043	0.000656	±0.000132	0.000012	±0.000027	9.03E-16	97.80%	6.4135	±5.29	6.42%
18	1.6	15	0.949433	±0.000915	±0.000455	0.001709	±0.000054	0.013232	±0.000221	0.000053	±0.000024	6.65E-15	98.49%	6.4997	±0.68	0.82%
19	1.7	15	0.193738	±0.000507	±0.000157	0.000294	±0.000034	-0.000280	±0.000315	0.000015	±0.000025	1.36E-15	97.76%	6.5834	±3.31	3.92%
20	1.8	10	0.048666	±0.000356	±0.000133	0.000079	±0.000034	0.000405	±0.000210	0.000026	±0.000020	3.41E-16	84.29%	5.4324	±10.43	14.91%

N: 10; P: % power of 60 W (60 W × (P/10) Synrad CO₂ laser; t: laser duration time; V: volts; %Rad: % radiogenic argon; R: ⁴⁰Ar*/³⁹Ar (Ar*: radiogenic argon); J: 0.0072827 ± 0.0000148 (1σ).

Table 9. Incremental heating ⁴⁰Ar/³⁹Ar dating of the sample 16D.

Steps	P	t	40 V	39 V	38 V	37 V	36 V	Moles ⁴⁰ Ar*	%Rad	R	Age (Ma)	%SD
1	0.5	15	0.155163 ±0.000494	0.025243 ±0.000130	0.000393 ±0.000041	0.000421 ±0.000219	0.000081 ±0.000022	1.09E-15	84.52%	5.1956	67.00 ±3.31	4.94%
2	0.6	15	0.244210 ±0.000423	0.037427 ±0.000134	0.000479 ±0.000049	0.000257 ±0.000167	0.000048 ±0.000020	1.71E-15	94.25%	6.1496	79.04 ±2.02	2.56%
3	0.6	15	0.166582 ±0.000458	0.026038 ±0.000129	0.000348 ±0.000048	0.000232 ±0.000167	0.000014 ±0.000020	1.17E-15	97.44%	6.2340	80.10 ±2.91	3.63%
4	0.6	15	0.796560 ±0.000622	0.119942 ±0.000362	0.001426 ±0.000058	-0.000319 ±0.000180	0.000101 ±0.000023	5.58E-15	96.26%	6.3927	82.10 ±0.78	0.95%
5	0.7	15	2.347745 ±0.001464	0.349089 ±0.000822	0.004408 ±0.000056	0.000917 ±0.000129	0.000298 ±0.000025	1.64E-14	96.25%	6.4732	83.10 ±0.34	0.41%
6	0.7	15	2.642274 ±0.001911	0.393495 ±0.000533	0.005225 ±0.000056	0.001013 ±0.000128	0.000283 ±0.000025	1.85E-14	96.84%	6.5025	83.47 ±0.28	0.33%
7	0.7	15	1.526283 ±0.001914	0.229127 ±0.000846	0.002918 ±0.000046	0.000477 ±0.000247	0.000130 ±0.000019	1.07E-14	97.48%	6.4935	83.36 ±0.46	0.55%
8	0.8	15	1.174862 ±0.001669	0.176048 ±0.000500	0.002152 ±0.000032	0.000277 ±0.000179	0.000119 ±0.000024	8.23E-15	97.01%	6.4741	83.12 ±0.59	0.71%
9	0.8	15	1.309897 ±0.001102	0.196614 ±0.000284	0.002515 ±0.000062	0.000515 ±0.000315	0.000150 ±0.000025	9.17E-15	96.63%	6.4377	82.66 ±0.51	0.61%
10	0.8	15	2.247964 ±0.001418	0.334557 ±0.000545	0.004160 ±0.000076	0.000968 ±0.000210	0.000231 ±0.000037	1.57E-14	96.97%	6.5155	83.64 ±0.45	0.53%
11	0.9	15	2.518615 ±0.001583	0.374885 ±0.000559	0.004709 ±0.000068	0.000391 ±0.000158	0.000296 ±0.000023	1.76E-14	96.53%	6.4855	83.26 ±0.27	0.33%
12	0.9	15	3.371300 ±0.002151	0.499839 ±0.000664	0.006607 ±0.000147	0.000659 ±0.000175	0.000378 ±0.000023	2.36E-14	96.69%	6.5215	83.71 ±0.22	0.26%
13	0.9	15	4.812822 ±0.003988	0.713168 ±0.001255	0.009113 ±0.000101	0.001278 ±0.000242	0.000532 ±0.000026	3.37E-14	96.74%	6.5282	83.80 ±0.22	0.26%
14	1.0	15	2.458399 ±0.001717	0.366830 ±0.000728	0.004651 ±0.000048	0.003824 ±0.000217	0.000259 ±0.000023	1.72E-14	96.90%	6.4940	83.37 ±0.30	0.36%
15	1.3	15	2.403995 ±0.001082	0.357096 ±0.000748	0.004713 ±0.000090	0.002728 ±0.000318	0.000291 ±0.000027	1.68E-14	96.43%	6.4921	83.34 ±0.34	0.41%
16	1.5	15	1.969217 ±0.001487	0.289955 ±0.000942	0.003592 ±0.000087	0.000850 ±0.000186	0.000233 ±0.000023	1.38E-14	96.51%	6.5546	84.13 ±0.42	0.50%
17	1.6	10	0.356726 ±0.000433	0.052932 ±0.000306	0.000596 ±0.000053	0.000096 ±0.000046	0.000055 ±0.000025	2.50E-15	95.43%	6.4310	82.58 ±1.88	2.27%

N: 10; P: % power of 60 W (60 W × (P/10) Synrad CO₂ laser; t: laser duration time; V: volts; %Rad: % radiogenic argon; R: ⁴⁰Ar*/³⁹Ar (Ar*: radiogenic argon); J: 0.00072827 ± 0.0000148 (1σ).

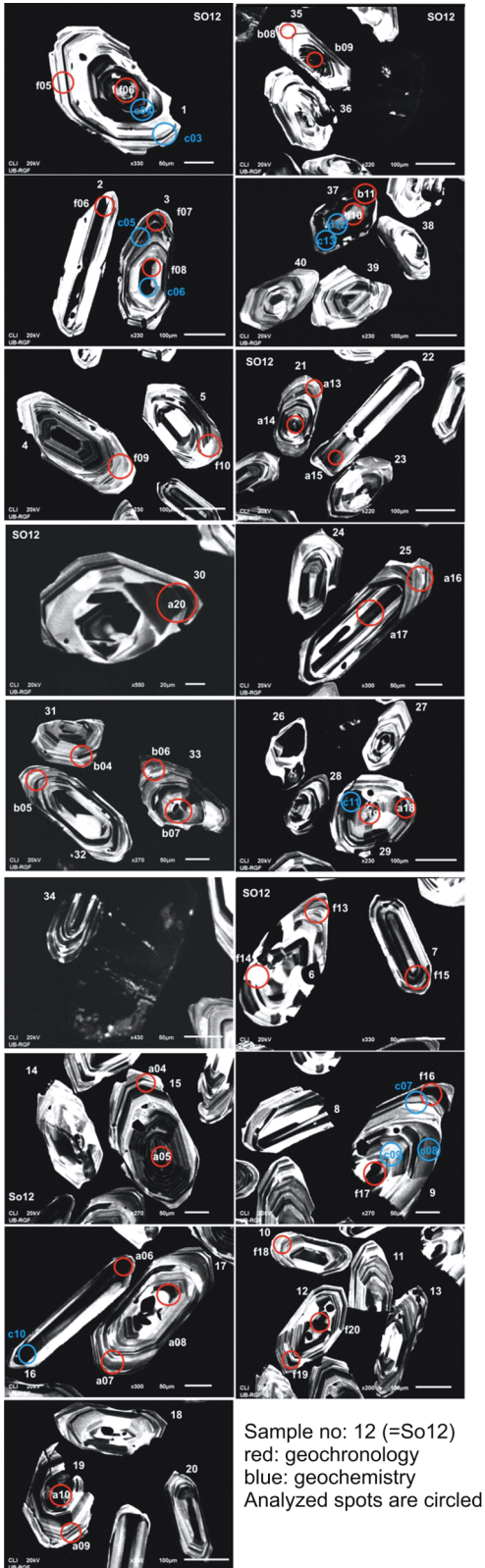


Figure 11. CL images of zircons from microgranodiorite (sample 12) of the Tavşanlı Zone. Spots used for geochronology and geochemistry are red and blue, respectively.

Based on existing and our new data, these $^{40}\text{Ar}/^{39}\text{Ar}$ ages could reflect phengite crystallization ages for the TZ and Alpine metamorphism that affected this zone can be constrained to approximately 83 Ma, corresponding to the Campanian. Comparing these ages obtained from schists, the results are consistent with other inferred ages for the TZ, metamorphosed in Campanian time as a result of northward subduction beneath the SZ, and the time of metamorphism gets younger to the south, from 83 Ma in the north to 63 Ma in the south (Özdamar et al., 2013).

The studied hypabyssal microgranodiorites have generally undergone weak alteration according to petrographic observations, and with 2.40 wt.% loss on ignition (LOI), we must take into account the influence of these events for further discussion. Metapelitic rocks of the TZ represent former shallow marine deposits metamorphosed in a subduction zone in the Late Cretaceous (~88 Ma) and subsequently involved in middle Eocene collision that resulted in the closure of the Neo-Tethys and intrusion. For these intrusive rocks, a previous hornblende $^{40}\text{Ar}/^{39}\text{Ar}$ age for the granitoid was estimated to be 53 ± 3 Ma (Harris et al., 1994; Sherlock et al., 1999), though the $^{40}\text{Ar}/^{39}\text{Ar}$ results could be interpreted to be too old in view of trapped extraneous argon in the hornblende. This earlier age estimate is consistent with an apatite fission-track age of 41.6 ± 4 Ma determined for the granitoid (Seaton et al., 2014). Our new zircon U-Pb age data revealed that the emplacement age of the hypabyssal microgranodiorites is 50.52 Ma, and we suggest this is a more precise and accurate representation of the crystallization age for the granitoids (Figure 12).

To reveal the thermal history of the Sivrihisar metamorphics and that the final stage of exhumation was accompanied by cooling, we applied different dating methods for different rocks. We could date metamorphism for the Sivrihisar metamorphic rock using $^{40}\text{Ar}/^{39}\text{Ar}$ dating. The only thermal event that we could date from the metamorphic rocks was HP/LT metamorphism, which happened ~83 Ma ago (Santonian) (providing constraint A in Figure 13). This time indicates the burial and related heating of the rocks at ~450 °C. Absence of sufficient crystal-sized zircon and apatite minerals in the metamorphic rocks did not allow us to evaluate the lower temperature thermal history of the metamorphic rocks. Instead, we dated a subvolcanic rock that was intruded into metamorphic rocks. The subvolcanic rock revealed ~51 Ma U-Pb zircon crystallization age (early Eocene) (Figure 13, constraint B). The Ti-in-zircon geothermometer (Claiborne et al., 2010) shows values in the range of 790–830 °C (see Table 10). Constraint C is represented by the late Eocene (U/Th)-He age of the apatites extracted from the subvolcanic rock. The closure temperature for the apatite (U/Th)-He system is presented as 65 ± 15 °C. This

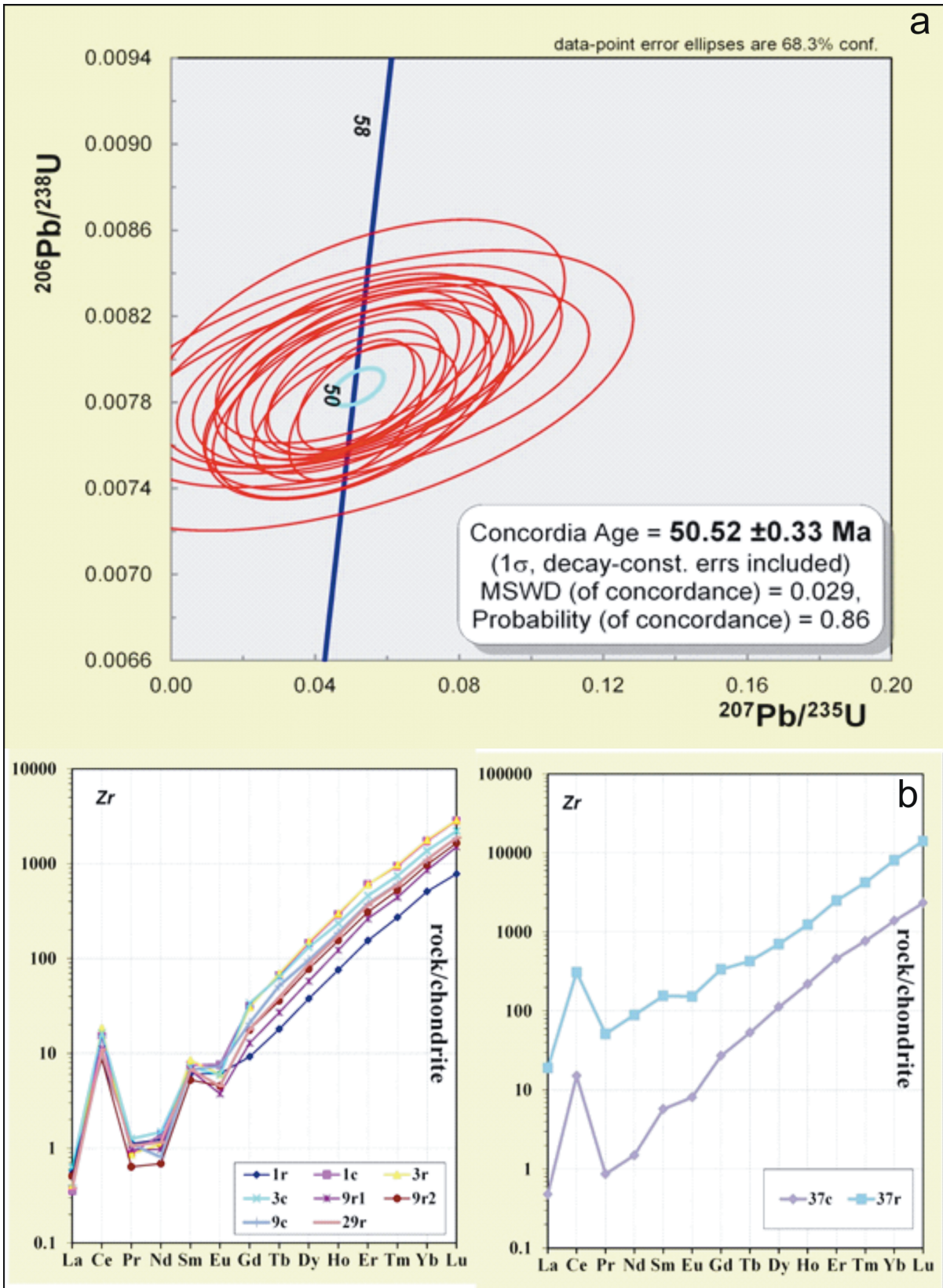


Figure 12. Geochronology and mineral chemistry of zircons from Sivrihisar granodiorite: a) Wetherill plot of LA U-Pb ages, b) chondrite-normalized REE patterns of zircon grains. The chondrite values are from Boynton (1984).

Table 10. Ti-in-zircon geothermometer values of zircon crystals from sample 12.

Sample 12	Ti (ppm)	Temperature (°C)
1r	18	832.20
1c	13	801.51
3r	14	802.95
3c	17	826.86
9r1	15	810.90
9r2	15	810.03
9c	16	818.45
29r	14	803.84
37c	12	790.25

near-surface exhumation of both units occurred at 38 Ma ago (Figure 13; Table 11).

Plunder et al. (2015) defined the P-T conditions for the TZ to be 24 kbar and ~500 °C on the basis of pseudosection modeling and Raman spectroscopy of carbonaceous material. Çetinkaplan et al. (2008) also described peak P-T conditions of lawsonite eclogites of 24 ± 1 kbar and 460 ± 25 °C for the Sivrihisar area. In this study, we estimated temperatures of about 303–484 °C and minimum pressures of 10 kbar for the TZ. These results are consistent with the P-T conditions of metamorphism inferred above. Thus, the age of Alpine metamorphism that affected the TZ can be constrained to be approximately 83 Ma, corresponding to the Campanian. Metamorphism dated along the sutures of the Neo-Tethys Ocean is generally attributed to either subduction of the Neo-Tethys Ocean under Eurasia or closure of the ocean and related regional metamorphism (Okay and Tüysüz, 1999; Özdamar et al., 2013). The

Table 11. AHe ages of apatite grains from sample 12.

Sample	He		U238			Th232			Th/U ratio	Sm			Ejection correct. (Ft)	Uncorr. He-age [Ma]	Ft-Corr. He-age [Ma]	2s [Ma]	2s [%]	Sample unweighted aver. ± 2 SE					
	Vol. [ncc]	1s [%]	Mass [ng]	1s [%]	Conc. [ppm]	Mass [ng]	1s [%]	Conc. [ppm]		Mass [ng]	1s [%]	Conc. [ppm]						[Ma]	[Ma]	[Ma]	[%]	[Ma]	[Ma]
	12	0.443	1.4	0.0641	2.0	11.8	0.211	2.4		38.9	3.3	0.7984						3.0	147.3	0.725	30.3	41.9	3.8
12	0.358	1.4	0.0532	2.1	10.1	0.1789	2.4	33.9	3.4	0.7616	3.0	144.4	0.706	29.0	41.1	4.0	9.7						
12	0.172	1.8	0.03	2.6	11.8	0.0988	2.5	38.8	3.3	0.3433	3.3	134.8	0.692	25.3	36.5	3.8	10.4						
12	0.387	1.4	0.059	2.1	11.0	0.2118	2.4	39.7	3.6	0.718	2.9	134.5	0.809	27.8	34.4	2.4	7.0	38.5	9.4				

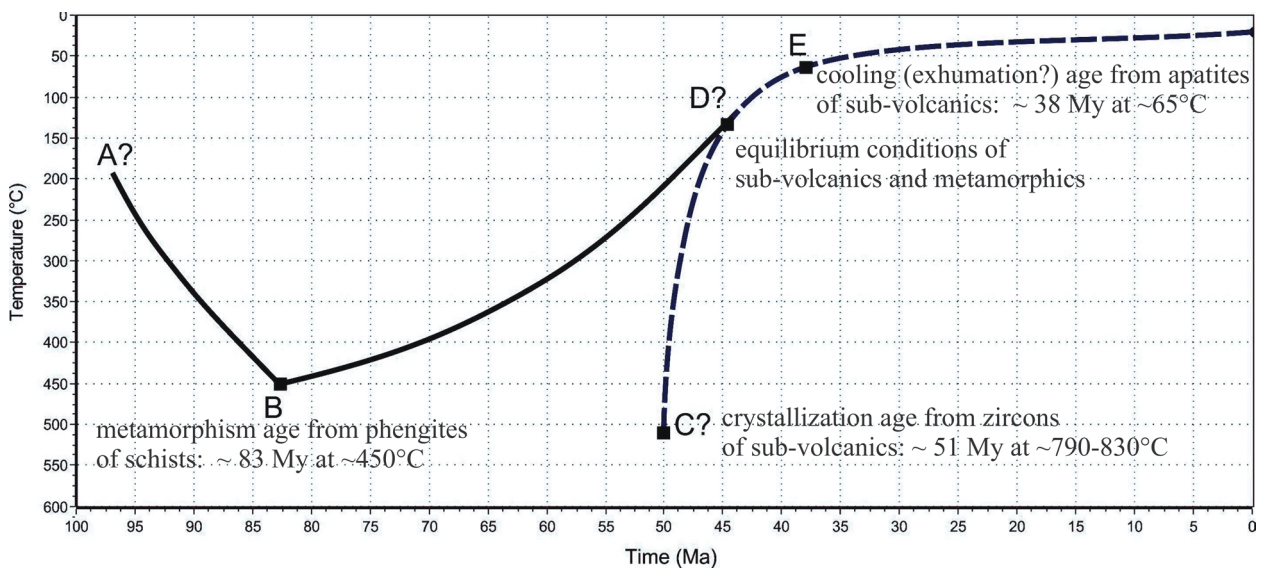


Figure 13. Temperature-time history for the Tavşanlı Zone constructed from muscovite-phengite ⁴⁰Ar/³⁹Ar, zircon U-Pb, and apatite (U-Th)/He age constraints.

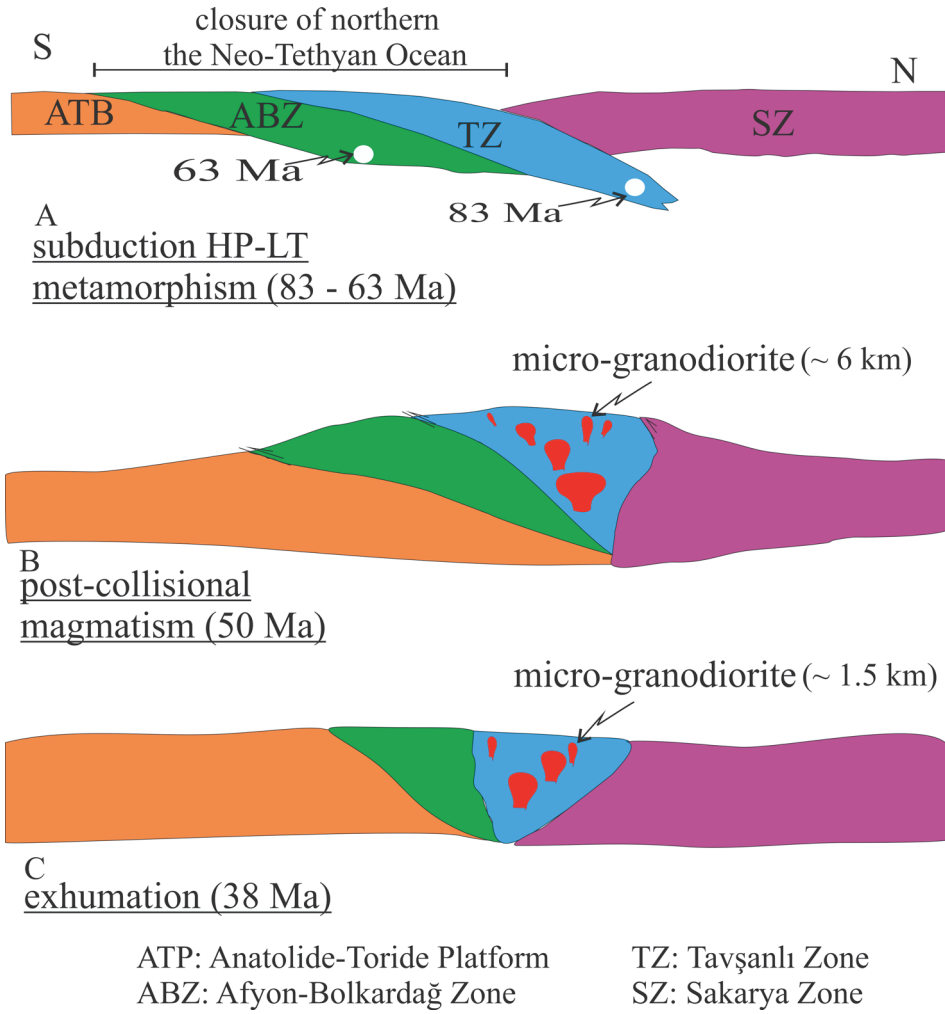


Figure 14. Schematic N-S cross-section explaining tectonics of the Tavşanlı Zone during Campanian to Bartonian times.

northern and southern branches of the Neo-Tethys Ocean have different histories (Şengör and Yılmaz, 1981). The timing of the subduction events of the Neo-Tethys Ocean is considered to be Upper Cretaceous for the northern branch (Okay and Tüysüz, 1999; Okay and Whitney, 2011; Özdamar et al., 2012; Özdamar et al., 2013) and Eocene for the southern one (Oberhänsli et al., 2012). All these data outlined above allow us to assert a tectonic model for this region (Figure 14). Therefore, northward subduction of the Neo-Tethyan ocean under the SZ occurred during the Campanian. In the Ypresina, the Sivrihisar granodiorite and microgranodiorite intruded into the metamorphic rocks. The exhumation of the hypabyssal rocks occurred 38 My ago.

6. Conclusions

We arrive at the following conclusions based on new data on the geology, whole-rock geochemistry, geochronology, and thermochronology.

1) The metamorphism of the pelitic, granitic, and basic rocks from the TZ occurred at around 83 Ma, corresponding approximately to the Campanian. This result is consistent with muscovite age data from metasedimentary rocks of the ABZ and could be related to the later stage of closure of the Neo-Tethys.

2) The P-T conditions of metamorphism is about 303–484 °C temperature and minimum 10 kbar pressure. This result is consistent with published data on metamorphism of the TZ.

3) Laser ablation ICP-MS U-Pb analyses of microgranodiorite gave 50 Ma. This age is interpreted as the formation age of the hypabyssal rocks as early Eocene time (Ypresian) in a compressional regime.

4) Apatite (U-Th)/He ages of the microgranodiorite gave 38 Ma, implying the exhumation age. This age also is interpreted such that the TZ had cooled to ~65 °C during the Bartonian.

Acknowledgments

This study was funded by an İTÜ-BAP project (Grant No. 36103). The authors are grateful to handling editor Orhan Karşlı for constructive notes on the manuscript. Fatih

Karaođlan and an anonymous reviewer are thanked for excellent comments that improved the scientific quality of the manuscript.

References

- Agard P, Monié P, Jolivet L, Goffé B (2002). Exhumation of the Schistes Lustrés complex: in situ laser probe Exhumation of the Schistes Lustrés Ar/Ar constraints and implications for the Western Alps. *J Metamorph Geol* 20: 599-618.
- Asiedu DK, Dampare SB, Sakyi PA, Banoeng-Yakubo B, Osae S, Nyarko BJB, Manu J (2004). Geochemistry of Paleoproterozoic metasedimentary rocks from the birim diamondiferous field, southern Ghana: implications for provenance and crustal evolution at the Archean-Proterozoic boundary. *Geochem J* 38: 215-228.
- Bebout GE (2007). Metamorphic chemical geodynamics of subduction zones. *Earth Planet Sc Lett* 260: 373-393.
- Bhatia M (1983). Plate tectonics and geochemical composition of sandstones. *J Geol* 91: 611-627.
- Bhatia MR, Crook KAW (1986). Trace element characteristics of graywackes and tectonic setting discrimination of sedimentary basins. *Contrib Mineral Petr* 92: 181-193.
- Bhattacharya A, Mohanty L, Maji A, Sen SK, Raith M (1992). Non-ideal mixing in the phlogopit-ennite binary: constraints from experimental data on Mg-Fe partitioning and a reformulation of the biotite-garnet geothermometer. *Contrib Mineral Petr* 111: 87-98.
- Boynnton WV (1984). Cosmochemistry of the rare earth elements: meteorite studies. In: Henderson R, editor. *Rare Earth Element Geochemistry. Developments in Geochemistry 2*. Amsterdam, the Netherlands: Elsevier, pp. 89-92.
- Candan O, Çetinkaplann M, Oberhänsli R, Rimmelé G, Akal C (2005). Alpine high-P/low-T metamorphism of the Afyon Zone and implications for the metamorphic evolution of Western Anatolia, Turkey. *Lithos* 84: 102-124.
- Çetinkaplan M, Candan O, Oberhänsli R, Bousquet R (2008). Pressure-temperature evolution of lawsonite eclogite in Sivrihisar; Tavşanlı Zone, Turkey. *Lithos* 104: 12-32.
- Claiborne LL, Miller CF, Wooden JL, Mazdab FK (2010). Trace element composition of igneous zircon: temporal, thermal, and compositional record of magmatic processes in the Spirit Mountain Batholith, Nevada. *Contrib Mineral Petr* 60: 511-531.
- Demirođlu M (2008). Hydrogeology and hydrochemistry of Eskişehir Sivrihisar-Günyüzü Basin. PhD, İstanbul Technical University, İstanbul, Turkey.
- Federico L, Capponi G, Crispini L, Scambelluri M, Villa IM (2005). ³⁹Ar/⁴⁰Ar dating of high-pressure rocks from the Ligurian Alps: evidence for a continuous subduction exhumation cycle. *Earth Planet Sc Lett* 240: 668-680.
- Ferry JM, Spear FS (1978). Experimental calibration of the partitioning of Fe and Mg between biotite and garnet. *Contrib Mineral Petr* 66: 113-117.
- Ganguly J, Saxena SK (1984). Mixing properties of aluminosilicate garnets: constraints from natural and experimental data, and application to geothermo-barometry. *Am Mineral* 69: 88-97.
- Girty GH, Barber RW (1993). REE, Th and Sc evidence for the depositional setting and source rock characteristics of the Quartz Hill chert. *Geol S Am S* 284: 109-119.
- Göncüođlu MC, Dirik K, Kozlu H (1997). General characteristics of pre-Alpine and Alpine Terranes in Turkey: explanatory notes to the terrane map of Turkey. *Annales Géologiques des Pays Helléniques* 37: 515-536.
- Hackler RT, Wood BJ (1989). Experimental determination of Fe and Mg exchange between garnet and olivine and estimation of Fe-Mg garnet mixing properties. *Am Mineral* 74: 994-999.
- Harris NBW, Kelley SP, Okay AI (1994). Post-collision magmatism and tectonics in northwest Turkey. *Contrib Mineral Petr* 117: 241-252.
- Hodges KV, Spear FS (1982). Geothermometry, geobarometry and the Al₂SiO₅ triple point at Mt. Moosilauke, New Hampshire. *Am Mineral* 67: 1118-1134.
- Holdaway MJ, Lee SM (1977). Fe-Ma cordierite stability in high grade pelitic rocks based on experimental, theoretical and natural observations. *Contrib Mineral Petr* 63: 175-198.
- Jackson S, Pearson N, Griffin W, Belousova E (2004). The application of laser ablation-inductively coupled plasma-mass spectrometry to in situ U-Pb zircon geochronology. *Chem Geol* 211: 47-69.
- Krogh EJ, Oh CW, Liou JG (1994). Polyphase and anticlockwise P-T evolution for Franciscan eclogites and blueschists from Jenner, California, USA. *J Metamorph Geol* 12: 121-34.
- Kulaksız S (1981). Sivrihisar kuzeybatı yöresinin jeolojisi. *Yerbilimleri* 8: 103-124 (in Turkish).
- Leake BE, Woolley AR, Arps CES (1997). Nomenclature of amphiboles: report of the Subcommittee on Amphiboles of the International Mineralogical Association commission on new minerals and mineral names. *Eur J Mineral* 9: 623-651.
- Ludwig KR (2003). *Isoplot/Ex Version 3.0: A Geochronological Toolkit for Microsoft Excel*. Berkeley, CA, USA: Berkeley Geochronology Center Special Publications.
- McLennan SM, Hemmin SR, Taylor SR, Eriksson KA (1995). Early Proterozoic crustal evolution: geochemical and Nd-Pb isotopic evidence from metasedimentary rocks, southern North America. *Geochim Cosmochim Acta* 59: 1153-1177.

- Norman MD, Griffin WL, Pearson NJ, Garcia MO, O'Reilly SY (1998). Quantitative Analysis of Trace Element Abundances in Glasses and Minerals: A Comparison of Laser Ablation ICPMS, Solution ICPMS, Proton Microprobe, and Electron Microprobe Data. Mineralogical Association of Canada Short Course 40. Vancouver, Canada: Mineralogical Association of Canada.
- Oberhänsli R, Bousquet R, Candan O, Okay AI (2012). Dating subduction events in East Anatolia. *Turkish J Earth Sci* 21: 1-18.
- Okay AI (1984). Distribution and characteristics of the northwest Turkish blueschists. *Geol Soc Spec Publ* 17: 455-466.
- Okay AI (1986). High pressure/low temperature metamorphic rocks of Turkey. *Geol Soc Am Mem* 164: 333-348.
- Okay AI (1989). Tectonic units and sutures in the Pontides, northern Turkey. In: Şengör AMC, editor. *Tectonic Evolution of the Tethyan Region*. Dordrecht, the Netherlands: Kluwer, pp. 109-116.
- Okay AI (2002). Jadeite-chloritoid-glaucophane-lawsonite schists from northwest Turkey: unusually high P/T ratios in continental crust. *J Metamorph Geol* 20: 757-768.
- Okay AI, Kelley SP (1994). Tectonic setting, petrology and geochronology of jadeite + glaucophane and chloritoid + glaucophane schists from northwest Turkey. *J Metamorph Geol* 12: 455-466.
- Okay AI, Tüysüz O (1999). Tethyan sutures of northern Turkey. *Geol Soc Spec Publ* 156: 475-515.
- Okay AI, Whitney DL (2011). Blueschists, eclogites, ophiolites and suture zones in northwest Turkey: a review and a field excursion guide. *Ofioliti* 35: 131-172.
- Örgün Tutay Y, Altınsoy N, Gültekin AH, Karahan G, Çelebi N (2005). Natural radioactivity levels in granitic plutons and groundwaters in Southeast part of Eskişehir Turkey. *Appl Radiat Isotopes* 63: 267-275.
- Özdamar Ş, Billor MZ, Sunal G, Esenli F, Roden MF (2013). First U-Pb SHRIMP zircon and $^{40}\text{Ar}/^{39}\text{Ar}$ ages of metarhyolites from the Afyon-Bolkardağ Zone, SW Turkey: implications for the rifting and closure of the Neo-Tethys. *Gondwana Res* 24: 377-391.
- Özdamar Ş, Roden MF, Esenli F, Uz B, Wampler JM (2012). Geochemistry and K-Ar ages of metasedimentary and metasomatized high-K metavolcanics rocks in the Afyon-Bolkardağ Zone (Ilgin-Konya), SW Turkey. *Neues Jb Miner Abh* 189: 155-176.
- Parra T, Vidal O, Agard P (2002). A thermodynamic model for Fe- Mg dioctahedral K white micas using data from phase equilibrium experiments and natural pelitic assemblages. *Contrib Mineral Petr* 143: 706-732.
- Perchuk LL, Lavrent'eva IV (1983). Experimental investigation of exchange equilibria in the system cordierite-garnet-biotite. In: Saxena SK, editor. *Kinetics and Equilibrium in Mineral Reactions*. New York, NY, USA: Springer, pp. 199-239.
- Plunder A, Agard P, Chopin C, Pourceau A, Okay AI (2015). Accretion, underplating and exhumation along a subduction interface: from subduction initiation to continental subduction (Tavşanlı zone, W. Turkey). *Lithos* 226: 233-254.
- Pourceau A, Sudo M, Candan O, Lanari P, Vidal O, Oberhänsli R (2013). Neotethys closure history of Anatolia: insights from $^{40}\text{Ar}/^{39}\text{Ar}$ geochronology and P-T estimation in high-pressure metasedimentary rocks. *J Metamorph Geol* 31: 585-606.
- Renne PR, Swisher CC, Deino AL, Karner DB, Owens T, DePaolo DJ (1998). Intercalibration of standards, absolute ages and uncertainties in $^{40}\text{Ar}/^{39}\text{Ar}$ dating. *Chem Geol* 145: 117-152.
- Robertson AHF, Parlak O, Ustaömer T (2009). Mélange and ophiolite emplacement related to subduction of the northern margin of the Tauride-Anatolide continent, central and western Turkey. *Geol Soc Spec Publ* 311: 9-66.
- Seaton NC, Whitney DL, Teyssier C, Toraman E, Heizler MT (2009). Recrystallization of high-pressure marble (Sivrihisar, Turkey). *Tectonophysics* 479: 241-253.
- Seaton NCA, Teyssier C, Whitney DL, Heizler MT (2014). Quartz and calcite microfabric transitions in a pressure and temperature gradient, Sivrihisar, Turkey. *Geodin Acta* 26: 191-206.
- Şengör AMC, Yılmaz Y (1981). Tethyan evolution of Turkey: a plate tectonic approach. *Tectonophysics* 75: 181-241.
- Sherlock S, Kelley SP, Inger S, Harris N, Okay AI (1999). ^{40}Ar - ^{39}Ar and Rb-Sr geochronology of high-pressure metamorphism and exhumation history of the Tavşanlı Zone, NW Turkey. *Contrib Mineral Petr* 137: 46-58.
- Silaupa S (2002). Rare-earth element geochemistry of Ordovician and Silurian shales in Lithuania: a provenance study. *Geologija* 37: 3-19.
- Sun SS, McDonough WF (1989). Chemical and isotopic systematics of ocean basalts: implications for mantle composition and processes. *Geol Soc Spec Publ* 42: 313-345.
- Taylor SR, McLennan SM (1985). *The Continental Crust: Its Composition and Evolution*. Oxford, UK: Blackwell Scientific.
- Thompson AB (1976). Mineral reactions in pelitic rocks. I. Prediction of P-T-X(Fe Mg) phase relations. II. Calculations of some P-T-X(Fe Mg) phase relations. *Am J Sci* 276: 425-454.
- Volkova NI, Stupakov SI, Babin GA, Rudnev SN, Mongush AA (2009). Mobility of trace elements during subduction metamorphism as exemplified by the blueschists of the Kurtushibinsky Range, Western Sayan. *Geochem Int* 47: 380-392.
- Whitney DL (2002). Coexisting andalusite, kyanite, and sillimanite: sequential formation of three Al_2SiO_5 polymorphs during progressive metamorphism near the triple point, Sivrihisar, Turkey. *Am Mineral* 87: 405-416.
- Whitney DL, Davis PB (2006). Why is lawsonite eclogite so rare? Metamorphism and preservation of lawsonite eclogite, Sivrihisar, Turkey. *Geology* 34: 473-476.
- Whitney DL, Teyssier C, Toraman E, Seaton NCA, Fayon AK (2011). Metamorphic and tectonic evolution of a structurally continuous blueschist-to-Barrovian terrane, Sivrihisar Massif, Turkey. *J Metamorph Geol* 29: 193-212.
- Wijbrans JR, McDougall I (1986). $^{40}\text{Ar}/^{39}\text{Ar}$ dating of white micas from an Alpine high pressure metamorphic belt on Naxos (Greece): the resetting of the argon isotopic system. *Contrib Mineral Petrol* 93: 187-194.